Electronic Research Archive

https://www.aimspress.com/journal/era

ERA, 34(5): 3223–3250.
DOI: 10.3934/era.2026145
Received: 16 January 2026
Revised: 25 February 2026
Accepted: 09 March 2026
Published: 14 April 2026

Research article

Energy-stable EIEQ time discretization for the PFC–FCC model: Convergence analysis and applications to crystal growth

Lianghong Yuan[1], **Haoyuan Wu**[2], **Yu Chen**[3], **Jun Zhang**[4,*] **and Xiaofeng Yang**[5,*]

[1] School of Mathematics and Statistics, Guizhou University of Finance and Economics, Guiyang 550025, China

[2] Moses Brown School, Providence, RI 02906, USA

[3] Graduate School of Business (GSB), SEGi University, Kota Damansara, Malaysia

[4] Computational Mathematics Research Center, Guizhou University of Finance and Economics, Guiyang 550025, China

[5] Department of Mathematics, University of South Carolina, Columbia, SC 29208, USA

* **Correspondence:** Email: jzhang@mail.gufe.edu.cn, xfyang@math.sc.edu.

Abstract: The phase-field crystal (PFC) model is widely used to describe atomic-scale crystalline patterns on diffusive time scales and to study the long-time evolution of microstructures. From the viewpoint of computational fluid dynamics, the standard two-mode PFC formulation for face-centered cubic ordering (PFC–FCC model) can be regarded as a high-order phase-field model for solid–liquid phase transitions, in which the motion of diffuse solid–liquid and grain boundaries is encoded in the evolution of a conserved order parameter. In this work, we constructed a linear, fully decoupled time-discretization scheme for the PFC-FCC system based on the explicit Invariant Energy Quadratization (EIEQ) approach. The scheme requires only the solution of constant-coefficient elliptic problems at each time step, making it well suited for fast solvers in large-scale simulations. We proved unique solvability, unconditional energy stability, and a rigorous optimal first-order a priori error estimate under suitable regularity assumptions, relying on a uniform L^∞-bound for the discrete density to control the nonlinear terms. Numerical tests with a manufactured solution confirmed the predicted convergence rate, while two- and three-dimensional simulations of solidification and crystallization with moving crystalline interfaces illustrated the stability, energy-dissipation property, and effectiveness of the EIEQ-based scheme as a numerical tool for long-time simulations of FCC/BCC pattern selection.

Keywords: error estimate; EIEQ; fully-decoupled; first-order; PFC-FCC; energy stability

1. Introduction

Microstructure evolution in crystalline materials, such as grain growth, phase transformations between competing crystal structures, and the formation and motion of defects, plays a central role in determining macroscopic properties, including strength, ductility, and resistance to fracture. Capturing these processes requires models that resolve atomic-scale periodicity while remaining efficient on the much longer time scales over which microstructures coarsen. The phase-field crystal (PFC) model, initially developed by Elder et al. in [1, 2], describes a coarse-grained atomic number density and, through an appropriate free-energy functional, accounts for elastic and plastic response, interfacial energy, and grain-boundary energetics. Because it resolves atomic length scales but evolves on diffusive time scales, the PFC framework can follow slow microstructural processes such as reconstructive phase transitions and spinodal decomposition that are essentially inaccessible to conventional molecular dynamics simulations [3]. It has been applied to a variety of crystal symmetries, such as body-centered cubic (BCC) and other simple lattices and tetragonal systems [4–8].

In this work, we are concerned with numerical schemes for close-packed structures, particularlly face-centered cubic (FCC) ordering. We use the standard two-mode PFC formulation for FCC structures (PFC–FCC model) [9], in which two sets of density waves are included in the free energy so that the FCC lattice is built into the model. This PFC-FCC framework has been used to study, for example, the competition between FCC and hexagonal close-packed (HCP) phases, the evolution of FCC and BCC crystals, and quantitative properties of metallic systems near melting [10–15]. Among common metallic crystal structures, FCC and HCP are prototypical close-packed arrangements, while BCC is more open; the two-mode PFC–FCC model incorporates the dominant FCC/HCP density modes and is therefore a natural tool for studying phase selection and microstructure evolution in close-packed alloys. It provides a minimal continuum description that retains an atomistic resolution of interfaces, stacking faults, and grain boundaries between competing crystalline phases. Furthermore, the PFC-FCC model can be viewed as a high-order phase-field description of solid–liquid phase transitions, in which moving solid–liquid interfaces and grain boundaries are represented in a diffuse manner through the evolution of a conserved density-like order parameter.

From a numerical point of view, the PFC-FCC model leads to a high-order, stiff, and strongly nonlinear gradient-flow system. The corresponding evolution equation can be regarded as a sixth-order nonlinear parabolic-type equation driven by the H^{-1}-gradient flow of a highly nonconvex free energy, so that high-frequency modes relax very rapidly while low-frequency modes evolve on much longer time scales. Straightforward explicit discretizations are subject to very severe time-step restrictions, while fully implicit schemes require the solution of large nonlinear coupled systems at each step. For long-time simulations of FCC ordering, one would therefore like time-stepping schemes that are linear, energy-stable and, as far as possible, decoupled, with a rigorous error analysis available. Various structure-preserving schemes have been proposed for PFC and related phase-field models, such as convex-splitting methods [16, 17], nonlocal Lagrange multiplier methods [18], higher-order implicit-explicit Runge-Kutta methods [19], and operator-splitting methods [20]. These methods are designed to respect, at the discrete level, key qualitative features of the continuum model, particularly energy dissipation and (in many cases) mass conservation, but the resulting algorithms may involve nonlinear iterations or variable-coefficient linear solves that become costly in large three-dimensional simulations.

In addition, energy-quadratization ideas, in particular the invariant energy quadratization (IEQ) and scalar auxiliary variable (SAV) approaches, have been extensively used to construct linear energy-stable schemes for PFC-type and related gradient-flow models [21–23]. For the two-mode PFC–FCC model considered here, SAV-based schemes with stabilization have been developed in [22], and an adaptive SAV scheme based on a variable-step second-order backward differentiation formula has been proposed together with an error estimate for the fully discrete method in [23]. These results confirm that, for the two-mode PFC-FCC system, constructing linear energy-stable schemes within the SAV framework is relatively standard and rigorous convergence analysis is achievable. By contrast, for the same two-mode PFC-FCC model, quadratization-based schemes of IEQ type have so far been studied mainly at the level of stability, and to the best of our knowledge, a systematic error analysis is lacking. Hence, the main aim of this study is to establish rigorous error estimates for the IEQ-type linear schemes developed in this work for this particular model. From a methodological point of view, this fills a gap between the SAV-based convergence results and the growing body of IEQ-based schemes that have so far been justified only by energy stability and numerical evidence.

The energy quadratization approach, provides a convenient framework for constructing linear structure-preserving schemes for gradient-flow problems. In the IEQ approach the nonlinear free energy is rewritten in terms of an auxiliary variable, which leads to linear schemes that satisfy a modified energy dissipation law [22, 24–28]. IEQ-type formulations have been used to design linear energy-stable schemes for several PFC and PFC-type models. The explicit-IEQ (EIEQ) method further adjusts the evolution of the auxiliary variable so that the resulting linear systems involve only constant-coefficient elliptic operators, while retaining an energy-dissipation structure at the discrete level; EIEQ schemes have been applied to various phase-field and phase-field crystal models, in particular to Allen-Cahn and Cahn-Hilliard-type equations [29]. Rigorous error analysis of EIEQ-based schemes has been carried out for Allen–Cahn-type equations; see, for example, [30]. To the best of our knowledge, however, EIEQ has not been combined with the standard two-mode PFC–FCC model, and corresponding error estimates for this higher-order system are not available. In particular, the presence of a high-order operator, multiple length scales, and strong nonlinearities makes it nontrivial to derive uniform bounds on the discrete solution and to close optimal-order error estimates within the EIEQ framework.

In this work, we apply the EIEQ time-discretization framework [30] to the standard two-mode PFC-FCC model and analyze the convergence of the resulting schemes. On the numerical side, we design linear schemes based on an EIEQ reformulation that are decoupled at each time step and involve only constant-coefficient elliptic problems, which makes them convenient to implement with fast solvers. On the analytical side, we prove that the proposed schemes are uniquely solvable, inherit a discrete energy-dissipation law, and admit rigorous a priori error estimates. Numerical experiments are presented to illustrate the accuracy and energy stability of the schemes for FCC-ordering dynamics. In this way, we obtain an EIEQ-based convergence theory for the standard two-mode PFC-FCC model, complementary to SAV-based results, and demonstrate that the proposed schemes can serve as efficient and reliable tools for long-time simulations of FCC/BCC microstructures in two and three dimensions.

The remainder of the paper is organized as follows. In Section 2 we recall the two-mode PFC–FCC model and its basic energy-dissipation structure. In Section 3, we introduce the EIEQ reformulation of the model and derive the corresponding fully discrete linear schemes, together with a brief discussion of their decoupled implementation. The stability and error analyses for the EIEQ-based schemes is

carried out in Section 4, where a key step is to establish uniform bounds on the discrete solution and to derive optimal-order error estimates. Numerical experiments for FCC-ordering problems are presented in Section 5, including two- and three-dimensional solidification tests that illustrate the accuracy and the robustness of the proposed schemes. Finally, Section 6 contains some concluding remarks and a brief discussion of possible extensions of this work.

2. The governing model and numerical scheme

2.1. The PFC-FCC model

We begin by introducing the notation. Let $\Omega \subset \mathbb{R}^d$ be a periodic domain and denote

$$L_1 = \Delta + 1, L_2 = \Delta + q^2, \tag{2.1}$$

where $q > 0$ is a given constant. The phase-field variable is denoted by $\phi(\mathbf{x}, t)$, and the double-well potential is given by

$$F(\phi) = \frac{1}{4}\phi^4 - \frac{\epsilon}{2}\phi^2, f(\phi) = F'(\phi), \tag{2.2}$$

with positive constant $\epsilon > 0$. Throughout, $(\cdot, \cdot)$ and $|\cdot|$ denote the $L^2(\Omega)$ inner product and norm, respectively.

The free energy of the PFC–FCC model is defined by

$$E(\phi) = \int_\Omega \frac{\phi}{2} L_1^2(L_2^2 + r^2)\phi d\boldsymbol{x} + F(\phi)d\boldsymbol{x}, \tag{2.3}$$

where r is a positive constant. The associated gradient-flow dynamics with mobility $M(\phi) \geq 0$ are

$$\phi_t = \nabla \cdot (M(\phi)\nabla\mu), \tag{2.4}$$

$$\mu = L_1^2(L_2^2 + r^2)\phi + f(\phi). \tag{2.5}$$

We next recall the energy dissipation law for (2.4) and (2.5) under periodic boundary conditions. Taking the L^2 inner product of (2.4) with $-\mu$ and integrating by parts, we obtain

$$-(\phi_t, \mu) = -(M(\phi)\nabla\mu, \nabla\mu) = \| \sqrt{M(\phi)}\nabla\mu\|^2. \tag{2.6}$$

On the other hand, taking the L^2 inner product of (2.5) with ϕ_t gives

$$\begin{aligned}(\mu, \phi_t) &= (L_1^2(L_2^2 + r^2)\phi + f(\phi), \phi_t) \\ &= \frac{1}{2}\frac{\mathrm{d}}{\mathrm{d}t}\int_\Omega (\phi L_1^2(L_2^2 + r^2)\phi)d\mathbf{x} + \frac{\mathrm{d}}{\mathrm{d}t}\int_\Omega F(\phi)d\boldsymbol{x},\end{aligned}$$

where we use integration by parts and the definitions of L_1 and L_2.

Combining (2.6) and (2.7), and using definition (2.3) of $E(\phi)$, we arrive at the energy-dissipation identity

$$\frac{\mathrm{d}}{\mathrm{d}t}E(\phi) = -\| \sqrt{M(\phi)}\nabla\mu\|^2 \leq 0. \tag{2.7}$$

2.2. The EIEQ scheme

To treat the nonlinear potential $F(\phi)$, within the explicit-IEQ (EIEQ) framework [30] and obtain linear systems with constant coefficients, we introduce an auxiliary variable that quadratizes the bulk energy.

Recall that the potential is given by $F(\phi)$. We take a stabilization parameter $S \geq 0$ and a constant $A > 0$, such that $F(x) - \frac{S}{2}x^2 + A > 0$ for any $x \in (-\infty, \infty)$, and define

$$V(\phi) = \sqrt{F(\phi) - \frac{S}{2}\phi^2 + A}, \tag{2.8}$$

$$W(\phi) = 2\frac{\mathrm{d}}{\mathrm{d}\phi}V(\phi) = \frac{f(\phi) - S\phi}{\sqrt{F(\phi) - \frac{S}{2}\phi^2 + A}}. \tag{2.9}$$

With this definition, one has $F(\phi) = V^2 + \frac{S}{2}\phi^2 - A$, so that the energy (2.3) can be equivalently written as

$$E(\phi, V) = \int_\Omega \frac{\phi}{2}L_1^2(L_2^2 + r^2)\phi d\boldsymbol{x} + \frac{S}{2}\|\phi\|^2 + \|V\|^2 - A|\Omega|.$$

Now we further define another nonlocal auxilary variable $B(t)$ such that $B(t)$ satisfy the following ODE

$$\begin{cases} B_t = (WV, \phi_t) - (W\phi_t, V), \\ B|_{t=0} = 1, \end{cases} \tag{2.10}$$

which implies a solution $B(t) \equiv 1$.

Hence, with the two variables V and B, we write the original systems (2.4) and (2.5) as follows:

$$\phi_t = \nabla \cdot (M(\phi)\nabla\mu), \tag{2.11}$$

$$\mu = L_1^2(L_2^2 + r^2)\phi + S\phi + BVW, \tag{2.12}$$

$$V_t = \frac{1}{2}BW\phi_t, \tag{2.13}$$

$$B_t = (WV, \phi_t) - (W\phi_t, V), \tag{2.14}$$

with the initial conditions as follows:

$$\phi|_{t=0} = \phi_0, V|_{t=0} = V_0 = V(\phi_0), B|_{t=0} = 1.$$

Note that, under the above initial conditions, the EIEQ reformulation (2.11)–(2.14) is equivalent to the original systems (2.4) and (2.5). Indeed, with $B(t) \equiv 1$, the chemical potential equation (2.12) reads

$$\mu = L_1^2(L_2^2 + r^2)\phi + S\phi + VW, \tag{2.15}$$

and the evolution equation for V reduces to

$$V_t = \frac{1}{2}W\phi_t. \tag{2.16}$$

Integrating (2.16) with respect to t and applying the initial conditions, one recovers V's definition in (2.8). Moreover, by (2.9), we have $VW = f(\phi) - S\phi$. Substituting this identity into (2.15) yields (2.5).

In parallel with the energy dissipation law for the original system, the modified EIEQ system also satisfies an energy-dissipation law. By taking the L^2 inner product of (2.11) with $-\mu$, of (2.12) with $-\phi_t$, and of (2.13) with $2V$, and by multiplying (2.14) by B and adding the resulting identities, we obtain

$$\frac{\mathrm{d}}{\mathrm{d}t}E(\phi, B, V) = -\| \sqrt{M(\phi)}\nabla\mu\|^2 \leq 0, \tag{2.17}$$

where

$$E(\phi, B, V) = \int_\Omega \frac{\phi}{2}L_1^2(L_2^2 + r^2)\phi d\boldsymbol{x} + \frac{S}{2}\|\phi\|^2 + \|V\|^2 + \frac{1}{2}|B|^2 - A|\Omega| - \frac{1}{2}.$$

Since $B \equiv 1$, and V is recovered in the form (2.8) by integrating (2.16), substituting these expressions into $E(\phi, B, V)$ reproduces the original energy functional (2.3).

Now, based on the EIEQ reformulation (2.11)–(2.14), we construct a time-discrete scheme. For a given positive integer N, let $\delta t = T/N$ be the time step and $t_m = m\delta t$ for $m = 0, 1, \ldots, N$. A first-order time-discrete scheme for (2.11)–(2.14) is defined as follows: Given $(\phi^m, \phi^{m-1}, V^m, B^m)$, we compute $(\phi^{m+1}, \mu^{m+1}, V^{m+1}, B^{m+1})$ from

$$\frac{\phi^{m+1} - \phi^m}{\delta t} = \nabla \cdot (M(\phi^m)\nabla\mu^{m+1}), \tag{2.18}$$

$$\mu^{m+1} = L_1^2(L_2^2 + r^2)\phi^{m+1} + S\phi^{m+1} + B^{m+1}W^m V^m, \tag{2.19}$$

$$\frac{V^{m+1} - V^m}{\delta t} = \frac{1}{2}B^{m+1}W^m\phi_t^\star, \tag{2.20}$$

$$\frac{B^{m+1} - B^m}{\delta t} = \frac{1}{\delta t}(W^m V^m, \phi^{m+1} - \phi^m) - (W^m\phi_t^\star, V^{m+1}), \tag{2.21}$$

where $\phi_t^\star = \frac{\phi^m - \phi^{m-1}}{\delta t}$, and $W^m = W(\phi^m)$.

Remark 2.1. *The first-order scheme* (2.18)–(2.21) *requires the starting values ϕ^1, V^1 , and B^1. These are computed by the following first-order initialization scheme:*

$$\frac{\phi^1 - \phi^0}{\delta t} = \nabla \cdot (M(\phi^0)\nabla\mu^1), \tag{2.22}$$

$$\mu^1 = L_1^2(L_2^2 + r^2)\phi^1 + S\phi^1 + B^1 W^0 V^0, \tag{2.23}$$

$$\frac{V^1 - V^0}{\delta t} = \frac{1}{2}B^0 W^0 \frac{\phi^1 - \phi^0}{\delta t}, \tag{2.24}$$

$$\frac{B^1 - B^0}{\delta t} = \frac{1}{\delta t}(W^0 V^0, \phi^1 - \phi^0) - (W^0\tfrac{\phi^1 - \phi^0}{\delta t}, V^0). \tag{2.25}$$

This startup step involves solving a coupled linear system for (ϕ^1, V^1, B^1), but the coupling appears only at this first time level and is therefore acceptable in practice. Once ϕ^1, V^1 , and B^1 have been obtained from this initialization step, the scheme (2.18)–(2.21) *is used for all subsequent time steps.*

Theorem 2.1. *The scheme* (2.18)–(2.21) *is unconditionally energy stable, i.e.,*

$$\mathcal{E}^{m+1} - \mathcal{E}^m \leq -\delta t\| \sqrt{M(\phi^m)}\nabla\mu^{m+1}\|^2, \tag{2.26}$$

where

$$\begin{aligned}\mathcal{E}^{m+1} = &\frac{1}{2}\|L_1L_2\phi^{m+1}\|^2 + \frac{r^2}{2}\|L_1\phi^{m+1}\|^2 + \frac{S}{2}\|\phi^{m+1}\|^2 \\ &+ \|V^{m+1}\|^2 + \frac{1}{2}|B^{m+1}|^2 - A|\Omega| - \frac{1}{2}.\end{aligned} \tag{2.27}$$

Proof. Taking the L^2 inner product of (2.18) with $-\delta t\mu^{m+1}$ gives

$$-(\phi^{m+1} - \phi^m,\ \mu^{m+1}) = \delta t\|\sqrt{M(\phi^m)}\nabla\mu^{m+1}\|^2. \tag{2.28}$$

Taking the L^2-inner product of (2.19) with $\phi^{m+1}-\phi^m$, and using $2a(a-b) = a^2-b^2+(a-b)^2$, we deduce

$$\begin{aligned}(\mu^{m+1},\ \phi^{m+1} - \phi^m) &= (L_1^2(L_2^2 + r^2)\phi^{m+1} + S\phi^{m+1} + B^{m+1}W^mV^m,\ \phi^{m+1} - \phi^m) \\ &= (L_1L_2\phi^{m+1},\ L_1L_2(\phi^{m+1} - \phi^m)) + r^2(L_1\phi^{m+1},\ L_1(\phi^{m+1} - \phi^m)) \\ &\quad + \frac{S}{2}\|\phi^{m+1}\|^2 - \frac{S}{2}\|\phi^m\|^2 + \frac{S}{2}\|\phi^{m+1} - \phi^m\|^2 + B^{m+1}(W^mV^m,\ \phi^{m+1} - \phi^m) \\ &= \frac{1}{2}\|L_1L_2\phi^{m+1}\|^2 - \frac{1}{2}\|L_1L_2\phi^m\|^2 + \frac{1}{2}\|L_1L_2(\phi^{m+1} - \phi^m)\|^2 + \frac{r^2}{2}\|L_1\phi^{m+1}\|^2 \\ &\quad - \frac{r^2}{2}\|L_1\phi^m\|^2 + \frac{r^2}{2}\|L_1(\phi^{m+1} - \phi^m)\|^2 + \frac{S}{2}\|\phi^{m+1}\|^2 - \frac{S}{2}\|\phi^m\|^2 \\ &\quad + \frac{S}{2}\|\phi^{m+1} - \phi^m\|^2 + B^{m+1}(W^mV^m,\ \phi^{m+1} - \phi^m).\end{aligned} \tag{2.29}$$

Taking the L^2-inner product of (2.20) with $2\delta tV^{m+1}$ yields

$$\|V^{m+1}\|^2 - \|V^m\|^2 + \|V^{m+1} - V^m\|^2 = \delta tB^{m+1}(W^m\phi_t^\star, V^{m+1}). \tag{2.30}$$

Multiplying (2.21) with δtB^{m+1}, we obtain

$$\begin{aligned}&\frac{1}{2}|B^{m+1}|^2 - \frac{1}{2}|B^m|^2 + \frac{1}{2}|B^{m+1} - B^m|^2 \\ &= B^{m+1}(W^mV^m, \phi^{m+1} - \phi^m) - \delta tB^{m+1}(W^m\phi_t^\star, V^{m+1}).\end{aligned} \tag{2.31}$$

By combining (2.28)–(2.31) and dropping the nonnegative terms on the left-hand side, we get

$$\begin{aligned}&\frac{1}{2}\|L_1L_2\phi^{m+1}\|^2 - \frac{1}{2}\|L_1L_2\phi^m\|^2 + \frac{r^2}{2}\|L_1\phi^{m+1}\|^2 - \frac{r^2}{2}\|L_1\phi^m\|^2 \\ &+ \frac{S}{2}\|\phi^{m+1}\|^2 - \frac{S}{2}\|\phi^m\|^2 + \|V^{m+1}\|^2 - \|V^m\|^2 + \frac{1}{2}|B^{m+1}|^2 - \frac{1}{2}|B^m|^2 \\ &\le -\delta t\|\sqrt{M(\phi^m)}\nabla\mu^{m+1}\|^2,\end{aligned} \tag{2.32}$$

which implies (2.26).

2.3. Implementation

At first sight, the fully discrete system (2.18)–(2.21) couples the four unknowns $(\phi^{m+1}, \mu^{m+1}, V^{m+1}, B^{m+1})$ and could be interpreted as requiring the solution of a large block system at

each time step. A key advantage of the EIEQ formulation is that this is not necessary. The scalar auxiliary variable B^{m+1} is spatially constant, and all elliptic operators in (2.18)–(2.21) have constant coefficients. As a result, we can rewrite the scheme in a fully decoupled form: Only a few independent constant-coefficient elliptic problems and scalar equations need to be solved at each time level. This contrasts with classical IEQ formulations, which often involve variable-coefficient elliptic operators; for the PFC-FCC model considered here, the EIEQ reformulation leads instead to constant-coefficient elliptic solutions and a simple decoupled implementation.

The following five steps describe the implementation of the proposed EIEQ scheme.

Step 1: Affine decomposition with respect to B^{m+1}.

We represent the dependence of ϕ^{m+1}, μ^{m+1} and V^{m+1} on the scalar B^{m+1} in the form

$$\begin{cases} \phi^{m+1} = \phi_1^{m+1} + B^{m+1}\phi_2^{m+1}, \\ \mu^{m+1} = \mu_1^{m+1} + B^{m+1}\mu_2^{m+1}, \\ V^{m+1} = V_1^{m+1} + B^{m+1}V_2^{m+1}. \end{cases} \tag{2.33}$$

Step 2: Decoupled elliptic problems for ϕ_1^{m+1} and ϕ_2^{m+1}.

Substituting the first two relations in (2.33) into (2.18) and (2.19) gives

$$\frac{(\phi_1^{m+1} + B^{m+1}\phi_2^{m+1}) - \phi^m}{\delta t} = \nabla \cdot (M(\phi^m)\nabla(\mu_1^{m+1} + B^{m+1}\mu_2^{m+1})), \tag{2.34}$$

$$\begin{aligned} \mu_1^{m+1} + B^{m+1}\mu_2^{m+1} &= L_1^2(L_2^2 + r^2)(\phi_1^{m+1} + B^{m+1}\phi_2^{m+1}) \\ &\quad + S(\phi_1^{m+1} + B^{m+1}\phi_2^{m+1}) + B^{m+1}W^m V^m. \end{aligned} \tag{2.35}$$

Separating the coefficients of B^{m+1} and the remaining terms, we obtain two independent linear systems:

$$\begin{cases} \phi_2^{m+1} - \delta t \nabla \cdot (M(\phi^m)\nabla\mu_2^{m+1}) = 0, \\ \mu_2^{m+1} = L_1^2(L_2^2 + r^2)\phi_2^{m+1} + S\phi_2^{m+1} + W^m V^m, \end{cases} \tag{2.36}$$

and

$$\begin{cases} \phi_1^{m+1} - \delta t \nabla \cdot (M(\phi^m)\nabla\mu_1^{m+1}) = \phi^m, \\ \mu_1^{m+1} = L_1^2(L_2^2 + r^2)\phi_1^{m+1} + S\phi_1^{m+1}. \end{cases} \tag{2.37}$$

Both systems are supplemented with periodic boundary conditions,

Moreover, since (2.36) and (2.37) are linear constant-coefficient elliptic problems, they can be solved efficiently and independently (for example by FFT-based solvers), and standard arguments guarantee the uniqueness of ϕ_1^{m+1} and ϕ_2^{m+1}.

Step 3: Explicit update for V_1^{m+1} and V_2^{m+1}.

Using the last relation in (2.33) in (2.20), we obtain

$$\frac{(V_1^{m+1} + B^{m+1}V_2^{m+1}) - V^m}{\delta t} = \frac{1}{2}B^{m+1}W^m\phi_t^\star, \tag{2.38}$$

which can be decomposed as

$$\begin{cases} V_1^{m+1} = V^m, \\ V_2^{m+1} = \dfrac{\delta t}{2}W^m\phi_t^\star. \end{cases} \tag{2.39}$$

The right-hand side in (2.39) are known, so V_1^{m+1} and V_2^{m+1} are obtained directly.

Step 4: Scalar equation for B^{m+1}.

To determine B^{m+1}, we substitute the first and third relations in (2.33) into (2.21) and obtain a scalar linear equation of the form

$$(\frac{1}{\delta t}+\chi_1)B^{m+1}=\frac{B^m}{\delta t}+\chi_2, \tag{2.40}$$

where

$$\begin{cases} \chi_1=-\frac{1}{\delta t}(W^mV^m,\phi_2^{m+1})+(W^m\phi_t^\star,V_2^{m+1}),\\ \chi_2=\frac{1}{\delta t}(W^mV^m,\phi_1^{m+1}-\phi^m)-(W^m\phi_t^\star,V_1^{m+1}). \end{cases} \tag{2.41}$$

To guarantee solvability, we need $\frac{1}{\delta t}+\chi_1\neq 0$. This follows from (2.36) and (2.39). Indeed, taking the L^2 inner product of (2.36) with $\frac{1}{\delta t}\mu_2^{m+1}$ and with $-\frac{1}{\delta t}\phi_2^{m+1}$ gives

$$\begin{aligned} \frac{1}{\delta t}(\phi_2^{m+1},\mu_2^{m+1})&=-\|\sqrt{M(\phi^m)}\nabla\mu_2^{m+1}\|^2,\\ -\frac{1}{\delta t}(\phi_2^{m+1},\mu_2^{m+1})&=-\frac{1}{\delta t}\|L_1L_2\phi^{m+1}\|^2+\frac{r^2}{\delta t}\|L_1\phi^{m+1}\|^2\\ &\quad-\frac{S}{\delta t}\|\phi_2^{m+1}\|^2-\frac{1}{\delta t}(W^mV^m,\phi_2^{m+1}). \end{aligned} \tag{2.42}$$

Combining these two equalities yields

$$-\frac{1}{\delta t}(W^mV^m,\phi_2^{m+1})=\frac{1}{\delta t}\|L_1L_2\phi^{m+1}\|^2+\frac{r^2}{\delta t}\|L_1\phi^{m+1}\|^2+\frac{S}{\delta t}\|\phi_2^{m+1}\|^2+\|\sqrt{M(\phi^m)}\nabla\mu_2^{m+1}\|^2\geq 0. \tag{2.43}$$

Moreover, taking the L^2 inner product of the second relation in (2.39) with V_2^{m+1} gives

$$(W^m\phi_t^\star,V_2^{m+1})=\frac{2}{\delta t}\|V_2^{m+1}\|^2\geq 0. \tag{2.44}$$

Adding (2.43) and (2.44), we obtain

$$-\frac{1}{\delta t}(W^mV^m,\phi_2^{m+1})+(W^m\phi_t^\star,V_2^{m+1})\geq 0. \tag{2.45}$$

so that $\chi_1\geq 0$ therefore, $\frac{1}{\delta t}+\chi_1\neq 0$. Thus, (2.40) has a unique solution.

Step 5: Recovery of (ϕ^{m+1},V^{m+1}).

Finally, ϕ^{m+1} and V^{m+1} are reconstructed from (2.33) once ϕ_i^{m+1}, V_i^{m+1} and B^{m+1} are obtained.

Remark 2.2. *To summarize, although the original scheme* (2.18)–(2.21) *appears to couple all unknowns, the presence of the scalar nonlocal variable B^{m+1} enables us to reformulate it as a fully decoupled procedure. At each time step, one only needs to solve a few independent constant-coefficient elliptic problems for ϕ_1^{m+1} and ϕ_2^{m+1} and a scalar linear equation for B^{m+1}, followed by explicit updates of V_1^{m+1} and V_2^{m+1}. In particular, no variable-coefficient elliptic systems arise. This is one of the major practical advantages of the EIEQ approach over the classical IEQ formulations,which places its computational complexity on a par with that of SAV-type schemes.*

Remark 2.3. *The EIEQ method proposed in our paper is constructed based on the "zero energy contribution" principle, which differs from the SAV method. This approach not only yields a linear and fully decoupled algorithm but is also applicable to constructing numerical schemes for multi-field coupling problems, whereas the conventional SAV method is suitable only for cases involving a single phase-field variable. For the model under consideration in this work, however, the EIEQ and SAV methods yield linear and decoupled numerical schemes.*

3. Error analysis

In this section, we derive temporal error estimates for the first-order scheme (2.18)–(2.21). Throughout the analysis, we use the notation $a \lesssim b$ to denote $a \leq Cb$ with a positive constant C independent of the time step δt and the time index m.

We collect the regularity assumptions on the exact solution. Let $\phi, V, \mu, \varsigma_t = \{\phi_t, V_t\}, \varsigma_{tt} = \{\phi_{tt}, V_{tt}\}$. We assume that the exact solution (ϕ, V, μ) satisfies

$$\begin{cases} \phi \in L^\infty(0,T;H^2(\Omega)) \cap L^\infty(0,T;W^{2,\infty}(\Omega)), \\ V \in L^\infty(0,T;W^{2,\infty}(\Omega)), \mu \in L^\infty(0,T;H^2(\Omega)), \\ \varsigma_t \in L^2(0,T;H^1(\Omega)) \cap L^\infty(0,T;L^\infty(\Omega)), \\ \varsigma_{tt} \in L^2(0,T;L^2(\Omega)). \end{cases} \tag{3.1}$$

We define the error functions by

$$\begin{cases} e_\phi^m = \phi(t_m) - \phi^m, e_\mu^m = \mu(t_m) - \mu^m, \\ e_B^m = B(t_m) - B^m, e_V^m = V(t_m) - V^m. \end{cases} \tag{3.2}$$

The associated local truncation errors of the first-order time discretization are given by

$$\begin{aligned} R_1^{m+1} &= \phi_t(t_{m+1}) - \tfrac{1}{\delta t}(\phi(t_{m+1}) - \phi(t_m)), \\ R_2^{m+1} &= V_t(t_{m+1}) - \tfrac{1}{\delta t}(V(t_{m+1}) - V(t_m)), \\ R_3^{m+1} &= B_t(t_{m+1}) - \tfrac{1}{\delta t}(B(t_{m+1}) - B(t_m)). \end{aligned} \tag{3.3}$$

Under the regularity assumptions (3.1), a Taylor expansion in time yields

$$\|R_1^{m+1}\| \lesssim \delta t, \|R_2^{m+1}\| \lesssim \delta t, \|R_3^{m+1}\| \lesssim \delta t. \tag{3.4}$$

To prepare for the global error analysis and to obtain uniform bounds on the discrete solution ϕ^m, we first establish the following lemma.

Lemma 3.1. *Assume that the following conditions hold:*

- *(i) For all $x \in (-\infty, \infty)$, $F(x) - \frac{S}{2}x^2 + A \geq A - d_1 > 0$, where d_1 is a constant;*
- *(ii) $F(x) \in C^4(-\infty, \infty)$;*
- *(iii) There exists a positive constant C_0, such that $\|\phi(t_k)\|_{L^\infty} \leq C_0$ for any k, and*

$$\max_{m \leq n}(\|\phi^m\|_{L^\infty}) \leq C_0. \tag{3.5}$$

Then there exists a positive constant C, such that

$$\|W(t_{m+1}) - W^m\| \le C\|\phi(t_{m+1}) - \phi^m\|, \tag{3.6}$$

Proof. We apply the intermediate value Theorem to derive

$$\begin{aligned}
&|W(t_{m+1}) - W^m| \\
&\quad = \Big|\frac{f(\phi(t_{m+1})) - S\phi(t_{m+1})}{\sqrt{F(\phi(t_{m+1})) - \frac{S}{2}\phi^2(t_{m+1}) + A}} - \frac{f(\phi^m) - S\phi^m}{\sqrt{F(\phi^m) - \frac{S}{2}(\phi^m)^2 + A}}\Big| \\
&\quad = \Big|\frac{(f(\phi(t_{m+1})) - S\phi(t_{m+1}))\sqrt{F(\phi^m) - \frac{S}{2}(\phi^m)^2 + A}}{\sqrt{F(\phi(t_{m+1})) - \frac{S}{2}\phi^2(t_{m+1}) + A}\sqrt{F(\phi^m) - \frac{S}{2}(\phi^m)^2 + A}}\cdot \\
&\qquad - \frac{(f(\phi^m) - S\phi^m)\sqrt{F(\phi(t_{m+1})) - \frac{S}{2}\phi^2(t_{m+1}) + A}}{\sqrt{F(\phi(t_{m+1})) - \frac{S}{2}\phi^2(t_{m+1}) + A}\sqrt{F(\phi^m) - \frac{S}{2}(\phi^m)^2 + A}}\Big| \\
&\quad \le \Big|\frac{(f(\phi(t_{m+1})) - S\phi(t_{m+1}))\Big(\sqrt{F(\phi^m) - \frac{S}{2}(\phi^m)^2 + A} - \sqrt{F(\phi(t_{m+1})) - \frac{S}{2}\phi^2(t_{m+1}) + A}\Big)}{\sqrt{F(\phi(t_{m+1})) - \frac{S}{2}\phi^2(t_{m+1}) + A}\sqrt{F(\phi^m) - \frac{S}{2}(\phi^m)^2 + A}} \\
&\qquad + \frac{\sqrt{F(\phi^m) - \frac{S}{2}(\phi^m)^2 + A}(f(\phi(t_{m+1})) - S\phi(t_{m+1}) - f(\phi^m) + S\phi^m)}{\sqrt{F(\phi(t_{m+1})) - \frac{S}{2}\phi^2(t_{m+1}) + A}\sqrt{F(\phi^m) - \frac{S}{2}(\phi^m)^2 + A}}\Big| \\
&\quad \le \frac{(C_1 + SC_0)(|f(\xi_1)| + SC_0)}{(A - d_1)^2}|\phi(t_{m+1}) - \phi^m| + \frac{C_1(|f'(\xi_2)| + S)}{A - d_1}|\phi(t_{m+1}) - \phi^m|,
\end{aligned} \tag{3.7}$$

where $\xi_i = \alpha_i\phi^m + (1 - \alpha_i)\phi(t_{m+1})$ with $i = 1, 2$ and $\alpha_{1,2} \in [0, 1]$. Note that (3.5) can ensure ξ_1 and ξ_2 are both uniformed bounded, hence, there exist a constant C such that (3.6) is valid.

We next derive the error estimates by mathematical induction. To this end we introduce

$$G^* = \max_{t\in[0,T]}\|\phi(t)\|_{L^\infty} + 1. \tag{3.8}$$

For notational convenience, we set $\epsilon = M = 1$. The following result on the uniform boundedness of ϕ^m for scheme (2.18)–(2.21) will be needed.

Lemma 3.2. *Assume that (i) for $x \in (-\infty, \infty)$, $F(x) - \frac{S}{2}x^2 + A \ge A - d_1 > 0$; (ii) $F(x) \in C^4(-\infty, \infty)$; (iii) the exact solution of* (2.11)–(2.14) *satisfies the regularity condition* (2.33)*. Then there exists a constant $\tau_0 > 0$ such that, if the time step $\delta t \le \tau_0$, the numerical solution $\{\phi^m\}_{m=0}^N$ of* (2.18)–(2.21) *satisfies*

$$\|\phi^m\|_{L^\infty} \le G^*, m = 0, 1, 2, \ldots, N. \tag{3.9}$$

Proof. We proceed by mathematical induction. For the first step $m = 0$, the bound $\|\phi^0\|_{L^\infty} \le G^*$ holds by the definition of G^*. Assume that for m with $0 \le m \le N - 1$ we have $\|\phi^m\|_{L^\infty} \le G^*$. We will show that $\|\phi^{m+1}\|_{L^\infty} \le G^*$ also holds.

By subtracting the time-discrete scheme (2.18)–(2.21) from the continuous system (2.11)–(2.14) at t_{m+1}, we obtain

$$\frac{e_\phi^{m+1}-e_\phi^m}{\delta t}+R_1^{m+1}=\Delta e_\mu^{m+1}, \tag{3.10}$$

$$e_\mu^{m+1}=L_1^2(L_2^2+r^2)e_\phi^{m+1}+S\,e_\phi^{m+1}+B(t_{m+1})W(t_{m+1})V(t_{m+1})-B^{m+1}W^mV^m, \tag{3.11}$$

$$\frac{e_V^{m+1}-e_V^m}{\delta t}+R_2^{m+1}=\frac{1}{2}B(t_{m+1})W(t_{m+1})\phi_t(t_{m+1})-\frac{1}{2}B^{m+1}W^m\phi_t^\star, \tag{3.12}$$

$$\begin{aligned}\frac{e_B^{m+1}-e_B^m}{\delta t}+R_3^{m+1}=&(W(t_{m+1})V(t_{m+1}),\phi_t(t_{m+1}))-\frac{1}{\delta t}(W^mV^m,\phi^{m+1}-\phi^m)\\&+(W^m\phi_t^\star,V^{m+1})-(W(t_{m+1})\phi_t(t_{m+1}),V(t_{m+1})).\end{aligned} \tag{3.13}$$

Taking the L^2-inner products of (3.10)–(3.12) with ω, ν and φ, respectively, we obtain

$$(\frac{e_\phi^{m+1}-e_\phi^m}{\delta t},\omega)=(\Delta e_\mu^{m+1},\omega)-(R_1^{m+1},\omega), \tag{3.14}$$

$$\begin{aligned}(e_\mu^{m+1},\nu)=&(L_1^2(L_2^2+r^2)e_\phi^{m+1},\nu)+S\,(e_\phi^{m+1},\nu)\\&+(B(t_{m+1})W(t_{m+1})V(t_{m+1})-B^{m+1}W^mV^m,\nu),\end{aligned} \tag{3.15}$$

$$(\frac{e_V^{m+1}-e_V^m}{\delta t},\varphi)=(\frac{1}{2}B(t_{m+1})W(t_{m+1})\phi_t(t_{m+1})-\frac{1}{2}B^{m+1}W^m\phi_t^\star,\varphi)-(R_2^{m+1},\varphi). \tag{3.16}$$

Then, by setting $\omega=2\delta t e_\mu^{m+1}$ in (3.14), we obtain

$$\begin{aligned}2(e_\phi^{m+1}-e_\phi^m,e_\mu^{m+1})&=2\delta t(\Delta e_\mu^{m+1},e_\mu^{m+1})-2\delta t(R_1^{m+1},e_\mu^{m+1})\\&=-2\delta t\|\nabla e_\mu^{m+1}\|^2-2\delta t(R_1^{m+1},e_\mu^{m+1}).\end{aligned} \tag{3.17}$$

By setting $\omega=2\delta t L_1^2(L_2^2+r^2)e_\mu^{m+1}$ in (3.14) again, we obtain

$$\begin{aligned}&2(e_\phi^{m+1}-e_\phi^m,L_1^2(L_2^2+r^2)e_\mu^{m+1})\\&\quad=2\delta t(\Delta e_\mu^{m+1},L_1^2(L_2^2+r^2)e_\mu^{m+1})-2\delta t(R_1^{m+1},L_1^2(L_2^2+r^2)e_\mu^{m+1})\\&\quad=2\delta t(\Delta e_\mu^{m+1},L_1^2L_2^2e_\mu^{m+1})+2\delta t(\Delta e_\mu^{m+1},L_1^2r^2e_\mu^{m+1})-2\delta t(R_1^{m+1},L_1^2(L_2^2+r^2)e_\mu^{m+1})\\&\quad=-2\delta t(L_1L_2\nabla e_\mu^{m+1},L_1L_2\nabla e_\mu^{m+1})-2r^2\delta t(L_1\nabla e_\mu^{m+1},L_1\nabla e_\mu^{m+1})\\&\qquad-2\delta t(R_1^{m+1},L_1^2(L_2^2+r^2)e_\mu^{m+1})\\&\quad=-2\delta t\|L_1L_2\nabla e_\mu^{m+1}\|^2-2r^2\delta t\|L_1\nabla e_\mu^{m+1}\|^2-2\delta t(R_1^{m+1},L_1^2(L_2^2+r^2)e_\mu^{m+1}).\end{aligned} \tag{3.18}$$

By setting $\omega=-2\delta t\Delta e_\mu^{m+1}$ in (3.14), we obtain

$$\begin{aligned}-(e_\phi^{m+1}-e_\phi^m,2\Delta e_\mu^{m+1})&=-2\delta t(\Delta e_\mu^{m+1},\Delta e_\mu^{m+1})+2\delta t(R_1^{m+1},\Delta e_\mu^{m+1})\\&=-2\delta t\|\Delta e_\mu^{m+1}\|^2+2\delta t(R_1^{m+1},\Delta e_\mu^{m+1}).\end{aligned} \tag{3.19}$$

By setting $\nu=2\delta t e_\mu^{m+1}$ in (3.15), we obtain

$$\begin{aligned}2\delta t\|e_\mu^{m+1}\|^2=&2\delta t(L_1^2(L_2^2+r^2)e_\phi^{m+1},e_\mu^{m+1})+2\delta tS\,(e_\phi^{m+1},e_\mu^{m+1})\\&+2\delta t(B(t_{m+1})W(t_{m+1})V(t_{m+1})-B^{m+1}W^mV^m,e_\mu^{m+1}).\end{aligned} \tag{3.20}$$

By setting $\nu = -2L_1^2(L_2^2 + r^2)(e_\phi^{m+1} - e_\phi^m)$ in (3.15), we get

$$\begin{aligned}
&-2(e_\mu^{m+1}, L_1^2(L_2^2 + r^2)(e_\phi^{m+1} - e_\phi^m)) \\
&\quad = -2(L_1^2(L_2^2 + r^2)e_\phi^{m+1}, L_1^2(L_2^2 + r^2)(e_\phi^{m+1} - e_\phi^m)) - 2S(e_\phi^{m+1}, L_1^2(L_2^2 + r^2)(e_\phi^{m+1} - e_\phi^m)) \\
&\qquad - 2(B(t_{m+1})W(t_{m+1})V(t_{m+1}) - B^{m+1}W^mV^m, L_1^2(L_2^2 + r^2)(e_\phi^{m+1} - e_\phi^m)) \\
&\quad = -(\|L_1^2(L_2^2 + r^2)e_\phi^{m+1}\|^2 - \|L_1^2(L_2^2 + r^2)e_\phi^m\|^2 + \|L_1^2(L_2^2 + r^2)(e_\phi^{m+1} - e_\phi^m)\|^2) \\
&\qquad - S(\|L_1L_2e_\phi^{m+1}\|^2 - \|L_1L_2e_\phi^m\|^2 + \|L_1L_2(e_\phi^{m+1} - e_\phi^m)\|^2 \\
&\qquad + r^2(\|L_1e_\phi^{m+1}\|^2 - \|L_1e_\phi^m\|^2 + \|L_1(e_\phi^{m+1} - e_\phi^m)\|^2)) \\
&\qquad - 2(B(t_{m+1})W(t_{m+1})V(t_{m+1}) - B^{m+1}W^mV^m, L_1^2(L_2^2 + r^2)(e_\phi^{m+1} - e_\phi^m)).
\end{aligned} \tag{3.21}$$

By setting $\nu = -(2e_\phi^{m+1} - 2e_\phi^m)$ in (3.15), we get

$$\begin{aligned}
&-(e_\mu^{m+1},\ 2e_\phi^{m+1} - 2e_\phi^m) \\
&\quad = -(L_1^2(L_2^2 + r^2)e_\phi^{m+1}, 2e_\phi^{m+1} - 2e_\phi^m) - S(e_\phi^{m+1}, 2e_\phi^{m+1} - 2e_\phi^m) \\
&\qquad - (B(t_{m+1})W(t_{m+1})V(t_{m+1}) - B^{m+1}W^mV^m,\ 2e_\phi^{m+1} - 2e_\phi^m) \\
&\quad = (L_1^2L_2^2e_\phi^{m+1},\ 2e_\phi^{m+1} - 2e_\phi^m) - r^2(L_1^2e_\phi^{m+1},\ 2e_\phi^{m+1} - 2e_\phi^m) - S(e_\phi^{m+1},\ 2e_\phi^{m+1} - 2e_\phi^m) \\
&\qquad - (B(t_{m+1})W(t_{m+1})V(t_{m+1}) - B^{m+1}W^mV^m,\ 2e_\phi^{m+1} - 2e_\phi^m) \\
&\quad = -(\|L_1L_2e_\phi^{m+1}\|^2 - \|L_1L_2e_\phi^m\|^2 + \|L_1L_2(e_\phi^{m+1} - e_\phi^m)\|^2) \\
&\qquad - r^2(\|L_1e_\phi^{m+1}\|^2 - \|L_1e_\phi^m\|^2 + \|L_1(e_\phi^{m+1} - e_\phi^m)\|^2) \\
&\qquad - S(\|e_\phi^{m+1}\|^2 - \|e_\phi^m\|^2 + \|e_\phi^{m+1} - e_\phi^m\|^2) \\
&\qquad - (B(t_{m+1})W(t_{m+1})V(t_{m+1}) - B^{m+1}W^mV^m, 2e_\phi^{m+1} - 2e_\phi^m).
\end{aligned} \tag{3.22}$$

By setting $\nu = 2\Delta(e_\phi^{m+1} - e_\phi^m)$ in (3.15), we get

$$\begin{aligned}
&(e_\mu^{m+1},\ 2\Delta(e_\phi^{m+1} - e_\phi^m)) \\
&\quad = (L_1^2(L_2^2 + r^2)e_\phi^{m+1}, 2\Delta(e_\phi^{m+1} - e_\phi^m)) + S(e_\phi^{m+1}, 2\Delta(e_\phi^{m+1} - e_\phi^m)) \\
&\qquad + (B(t_{m+1})W(t_{m+1})V(t_{m+1}) - B^{m+1}W^mV^m,\ 2\Delta(e_\phi^{m+1} - e_\phi^m)) \\
&\quad = -2(L_1L_2\nabla e_\phi^{m+1}, L_1L_2\nabla(e_\phi^{m+1} - e_\phi^m)) - 2r^2(L_1\nabla e_\phi^{m+1}, L_1\nabla(e_\phi^{m+1} - e_\phi^m)) \\
&\qquad - 2S(\nabla e_\phi^{m+1}, \nabla(e_\phi^{m+1} - e_\phi^m)) \\
&\qquad + (B(t_{m+1})W(t_{m+1})V(t_{m+1}) - B^{m+1}W^mV^m, \Delta(e_\phi^{m+1} - e_\phi^m)) \\
&\quad = -(\|L_1L_2\nabla e_\phi^{m+1}\|^2 - \|L_1L_2\nabla e_\phi^m\|^2 + \|L_1L_2\nabla(e_\phi^{m+1} - e_\phi^m)\|^2) \\
&\qquad - r^2(\|L_1\nabla e_\phi^{m+1}\|^2 - \|L_1\nabla e_\phi^m\|^2 + \|L_1\nabla(e_\phi^{m+1} - e_\phi^m)\|^2) \\
&\qquad - S(\|\nabla e_\phi^{m+1}\|^2 - \|\nabla e_\phi^m\|^2 + \|\nabla(e_\phi^{m+1} - e_\phi^m)\|^2) \\
&\qquad + 2(B(t_{m+1})W(t_{m+1})V(t_{m+1}) - B^{m+1}W^mV^m, \Delta(e_\phi^{m+1} - e_\phi^m)).
\end{aligned} \tag{3.23}$$

By setting $\varphi = 4\delta t e_V^{m+1}$ in (3.16), we obtain

$$\begin{aligned}
&2(\|e_V^{m+1}\|^2 - \|e_V^m\|^2 + \|e_V^{m+1} - e_V^m\|^2) \\
&\qquad = 2\delta t(B(t_{m+1})W(t_{m+1})\phi_t(t_{m+1}) - B^{m+1}W^m\phi_t^\star, e_V^{m+1}) - 4\delta t(R_2^{m+1}, e_V^{m+1}).
\end{aligned} \tag{3.24}$$

Multiplying (3.13) with $2\delta t e_B^{m+1}$, we obtain

$$\begin{aligned}
&|e_B^{m+1}|^2 - |e_B^m|^2 + |e_B^{m+1} - e_B^m|^2 \\
&\qquad = -2\delta t e_B^{m+1} \cdot R_3^{m+1} + 2\delta t e_B^{m+1} \cdot (V(t_{m+1})W(t_{m+1}), \phi_t(t_{m+1})) \\
&\qquad\quad - 2e_B^{m+1} \cdot (W^m V^m, \phi^{m+1} - \phi^m) + 2\delta t e_B^{m+1} \cdot (W^m \phi_t^\star, V^{m+1}) \\
&\qquad\quad - 2\delta t e_B^{m+1} \cdot (W(t_{m+1})\phi_t(t_{m+1}), V(t_{m+1})).
\end{aligned} \tag{3.25}$$

Combining (3.17)–(3.25), we obtain

$$\begin{aligned}
&\|L_1L_2e_\phi^{m+1}\|^2 - \|L_1L_2e_\phi^m\|^2 + \|L_1L_2(e_\phi^{m+1} - e_\phi^m)\|^2 + r^2(\|L_1e_\phi^{m+1}\|^2 - \|L_1e_\phi^m\|^2 + \|L_1(e_\phi^{m+1} - e_\phi^m)\|^2) \\
&\quad + S(\|e_\phi^{m+1}\|^2 - \|e_\phi^m\|^2 + \|e_\phi^{m+1} - e_\phi^m\|^2) \\
&\quad + \|L_1^2(L_2^2 + r^2)e_\phi^{m+1}\|^2 - \|L_1^2(L_2^2 + r^2)e_\phi^m\|^2 + \|L_1^2(L_2^2 + r^2)(e_\phi^{m+1} - e_\phi^m)\|^2 \\
&\quad + S(\|L_1L_2e_\phi^{m+1}\|^2 - \|L_1L_2e_\phi^m\|^2 + \|L_1L_2(e_\phi^{m+1} - e_\phi^m)\|^2 \\
&\quad + r^2(\|L_1e_\phi^{m+1}\|^2 - \|L_1e_\phi^m\|^2 + \|L_1(e_\phi^m - e_\phi^{m+1})\|^2)) \\
&\quad + \|L_1L_2\nabla e_\phi^{m+1}\|^2 - \|L_1L_2\nabla e_\phi^m\|^2 + \|L_1L_2\nabla(e_\phi^{m+1} - e_\phi^m)\|^2 \\
&\quad + r^2(\|L_1\nabla e_\phi^{m+1}\|^2 - \|L_1\nabla e_\phi^m\|^2 + \|L_1\nabla(e_\phi^{m+1} - e_\phi^m)\|^2) \\
&\quad + S(\|\nabla e_\phi^{m+1}\|^2 - \|\nabla e_\phi^m\|^2 + \|\nabla(e_\phi^{m+1} - e_\phi^m)\|^2) \\
&\quad + 2(\|e_V^{m+1}\|^2 - \|e_V^m\|^2 + \|e_V^{m+1} - e_V^m\|^2) \\
&\quad + |e_B^{m+1}|^2 - |e_B^m|^2 + |e_B^{m+1} - e_B^m|^2 + 2\delta t\|\nabla e_\mu^{m+1}\|^2 + 2\delta t\|L_1L_2\nabla e_\mu^{m+1}\|^2 \\
&\quad + 2\delta t\|e_\mu^{m+1}\|^2 + 2r^2\delta t\|L_1\nabla e_\mu^{m+1}\|^2 + 2\delta t\|\Delta e_\mu^{m+1}\|^2 \\
&= -2\delta t(R_1^{m+1}, e_\mu^{m+1}) - 2\delta t(R_1^{m+1}, L_1^2(L_2^2 + r^2)e_\mu^{m+1}) - 4\delta t(R_2^{m+1}, e_V^{m+1}) - 2\delta t e_B^{m+1} \cdot R_3^{m+1} \\
&\quad + 2\delta t(R_1^{m+1}, \Delta e_\mu^{m+1}) + 2\delta t(L_1^2(L_2^2 + r^2)e_\phi^{m+1}, e_\mu^{m+1}) + 2\delta t S(e_\phi^{m+1}, e_\mu^{m+1}) \\
&\quad - 2(B(t_{m+1})W(t_{m+1})V(t_{m+1}) - B^{m+1}W^mV^m, e_\phi^{m+1} - e_\phi^m) \quad (\text{: } \mathbf{term\ I_1}) \\
&\quad - 2(B(t_{m+1})W(t_{m+1})V(t_{m+1}) - B^{m+1}W^mV^m, L_1^2(L_2^2 + r^2)(e_\phi^{m+1} - e_\phi^m)) \quad (\text{: } \mathbf{term\ I_2}) \\
&\quad + 2\delta t(B(t_{m+1})W(t_{m+1})V(t_{m+1}) - B^{m+1}W^mV^m, e_\mu^{m+1}) \quad (\text{: } \mathbf{term\ I_3}) \\
&\quad + 2\delta t(B(t_{m+1})W(t_{m+1})\phi_t(t_{m+1}) - B^{m+1}W^m\phi_t^\star, e_V^{m+1}) \\
&\quad + 2\delta t e_B^{m+1} \cdot (W^m\phi_t^\star, V^{m+1}) - 2\delta t e_B^{m+1} \cdot (W(t_{m+1})\phi_t(t_{m+1}), V(t_{m+1})) \quad (\text{: } \mathbf{term\ I_4}) \\
&\quad + 2\delta t e_B^{m+1} \cdot (V(t_{m+1})W(t_{m+1}), \phi_t(t_{m+1})) - 2e_B^{m+1} \cdot (W^mV^m, \phi^{m+1} - \phi^m) \quad (\text{: } \mathbf{term\ I_5}) \\
&\quad + 2(B(t_{m+1})W(t_{m+1})V(t_{m+1}) - B^{m+1}W^mV^m, \Delta(e_\phi^{m+1} - e_\phi^m)). \quad (\text{: } \mathbf{term\ I_6})
\end{aligned} \tag{3.26}$$

We estimate the terms on the right-hand side of (3.26) as follows. Using the Cauchy-Schwarz inequality, we obtain

$$-2\delta t(R_1^{m+1}, e_\mu^{m+1}) \lesssim \delta t\|R_1^{m+1}\|^2 + \delta t\|e_\mu^{m+1}\|^2, \tag{3.27}$$

$$-2\delta t(R_1^{m+1}, L_1^2(L_2^2 + r^2)e_\mu^{m+1}) \lesssim \delta t\|L_1^2(L_2^2 + r^2)R_1^{m+1}\|^2 + \delta t\|e_\mu^{m+1}\|^2, \tag{3.28}$$

$$-4\delta t(R_2^{m+1}, e_V^{m+1}) \lesssim \delta t\|R_2^{m+1}\|^2 + \delta t\|e_V^{m+1}\|^2, \tag{3.29}$$

$$-2\delta t e_B^{m+1}\cdot R_3^{m+1} \lesssim \delta t|e_B^{m+1}|^2+\delta t\|R_3^{m+1}\|^2, \tag{3.30}$$

$$2\delta t(R_1^{m+1},\Delta e_\mu^{m+1}) \lesssim \delta t\|\nabla R_1^{m+1}\|^2+\delta t\|\nabla e_\mu^{m+1}\|^2, \tag{3.31}$$

$$2\delta t(L_1^2(L_2^2+r^2)e_\phi^{m+1},e_\mu^{m+1}) \lesssim \delta t\|e_\mu^{m+1}\|^2+\delta t\|L_1^2(L_2^2+r^2)e_\phi^{m+1}\|^2, \tag{3.32}$$

and

$$2\delta t S(e_\phi^{m+1},e_\mu^{m+1}) \lesssim \delta t\|e_\phi^{m+1}\|^2+\delta t\|e_\mu^{m+1}\|^2. \tag{3.33}$$

We further estimate term $\mathbf{I_1}$. Note that

$$\begin{aligned} &B(t_{m+1})V(t_{m+1})W(t_{m+1})-B^{m+1}V^mW^m\\ &\quad=B(t_{m+1})\Big(V(t_{m+1})W(t_{m+1})-V^mW^m\Big)+e_B^{m+1}V^mW^m\\ &\quad=V(t_{m+1})(W(t_{m+1})-W^m)+(V(t_{m+1})-V^m)W^m+e_B^{m+1}V^mW^m, \end{aligned} \tag{3.34}$$

and

$$\begin{aligned} &B(t_{m+1})W(t_{m+1})\phi_t(t_{m+1})-B^{m+1}W^m\phi_t^*\\ &\quad=B(t_{m+1})\Big(W(t_{m+1})\phi_t(t_{m+1})-W^m\phi_t^*\Big)+e_B^{m+1}W^m\phi_t^*\\ &\quad=(W(t_{m+1})-W^m)\phi_t(t_{m+1})+W^m(\phi_t(t_{m+1})-\phi_t^*)+e_B^{m+1}W^m\phi_t^*, \end{aligned} \tag{3.35}$$

where

$$\begin{aligned} \phi_t(t_{m+1})-\phi_t^* &= R_1^{m+1}+\frac{\phi(t_{m+1})-\phi(t_m)}{\delta t}-\frac{\phi(t_m)-\phi(t_{m-1})}{\delta t}+\frac{e_\phi^m-e_\phi^{m-1}}{\delta t}\\ &= R_1^{m+1}+\frac{\phi(t_{m+1})-2\phi(t_m)+\phi(t_{m-1})}{\delta t}+\Delta e_\mu^m-R_1^m, \end{aligned} \tag{3.36}$$

where $\frac{\phi(t_{m+1})-2\phi(t_m)+\phi(t_{m-1})}{\delta t}=\mathcal{O}(\delta t)$, which is consistent with the results in [30].

Using Lemma 3.1 and (3.34), the term $\mathbf{I_1}$ can be estimated as

$$\begin{aligned} |\mathbf{I_1}| &= \Big|2\Big(B(t_{m+1})V(t_{m+1})W(t_{m+1})-B^{m+1}V^mW^m,e_\phi^{m+1}-e_\phi^m\Big)\Big|\\ &= 2\delta t\Big|\Big(V(t_{m+1})(W(t_{m+1})-W^m)+(V(t_{m+1})-V^m)W^m+e_B^{m+1}V^mW^m,\Delta e_\mu^{m+1}-R_1^{m+1}\Big)\Big|\\ &\lesssim \delta t\Big(\|V(t_{m+1})\|_{L^\infty}\|W(t_{m+1})-W^m\|+\|W^m\|_{L^\infty}\|V(t_{m+1})-V^m\|\\ &\quad+|e_B^{m+1}|\|V^m\|_{L^\infty}\|W^m\|_{L^\infty}\Big)\Big(\|\Delta e_\mu^{m+1}\|+\|R_1^{m+1}\|\Big)\\ &\lesssim \delta t\Big(\|W(t_{m+1})-W^m\|^2+\|V(t_{m+1})-V^m\|^2+|e_B^{m+1}|^2+\frac{1}{5}\|\Delta e_\mu^{m+1}\|^2+\|R_1^{m+1}\|^2\Big)\\ &\lesssim \delta t\Big(|e_B^{m+1}|^2+\|\phi(t_{m+1})-\phi^m\|^2+\frac{1}{5}\|\Delta e_\mu^{m+1}\|^2+\|R_1^{m+1}\|^2\Big)\\ &\lesssim \delta t(\delta t^2+|e_B^{m+1}|^2+\|e_\phi^m\|^2+\frac{1}{5}\|\Delta e_\mu^{m+1}\|^2), \end{aligned} \tag{3.37}$$

where $\|V^m\|_{L^\infty}, \|W^m\|_{L^\infty}, \|\Delta V^m\|_{L^\infty}, \|\Delta W^m\|_{L^\infty}$ are bounded since $\|\phi^m\|_{L^\infty}, \|\Delta\phi^m\|_{L^\infty}$ are bounded.

Similarly, applying Lemma 3.1 together with (3.35) and (3.36), we obtain analogous bounds for $|\mathbf{I_2}|$, $|\mathbf{I_3}|$, $|\mathbf{I_4}|$, $|\mathbf{I_5}|$, and $|\mathbf{I_6}|$, as follows:

$$\begin{aligned}
|\mathbf{I_2}| &= \Big|2\Big(B(t_{m+1})W(t_{m+1})V(t_{m+1}) - B^{m+1}W^mV^m, L_1^2(L_2^2+r^2)(e_\phi^{m+1}-e_\phi^m)\Big)\Big| \\
&= 2\delta t\Big|\Big(B(t_{m+1})W(t_{m+1})V(t_{m+1}) - B^{m+1}W^mV^m, L_1^2(L_2^2+r^2)(\Delta e_\mu^{m+1} - R_1^{m+1})\Big)\Big| \\
&= 2\delta t\Big|\Big(L_1^2(L_2^2+r^2)(B(t_{m+1})W(t_{m+1})V(t_{m+1}) - B^{m+1}W^mV^m), \Delta e_\mu^{m+1}\Big) \\
&\quad - \Big(B(t_{m+1})W(t_{m+1})V(t_{m+1}) - B^{m+1}W^mV^m, L_1^2(L_2^2+r^2)R_1^{m+1}\Big)\Big| \\
&\lesssim \delta t\Big(\delta t^2 + |e_B^{m+1}|^2 + \|e_\phi^m\| + \|L_1^2(L_2^2+r^2)e_\phi^m\| + \frac{1}{5}\|\Delta e_\mu^{m+1}\|^2\Big),
\end{aligned} \tag{3.38}$$

$$\begin{aligned}
|\mathbf{I_3}| &= 2\delta t\Big|\Big(B(t_{m+1})W(t_{m+1})V(t_{m+1}) - B^{m+1}W^mV^m, e_\mu^{m+1}\Big)\Big| \\
&= 2\delta t\Big(\|W(t_{m+1}) - W^m\| + \|V(t_{m+1}) - V^m\| + |e_B^{m+1}|\Big)\cdot\|e_\mu^{m+1}\| \\
&\lesssim \delta t\Big(\delta t^2 + \|e_\phi^m\|^2 + |e_B^{m+1}|^2 + \|e_\mu^{m+1}\|^2\Big),
\end{aligned} \tag{3.39}$$

$$\begin{aligned}
|\mathbf{I_4}| = &\Big|2\delta t\Big(B(t_{m+1})W(t_{m+1})\phi_t(t_{m+1}) - B^{m+1}W^m\phi_t^\star, e_V^{m+1}\Big) \\
&+ 2\delta t e_B^{m+1}\Big(W^m\phi_t^\star, V^{m+1}\Big) - 2\delta t e_B^{m+1}\Big(W(t_{m+1})\phi_t(t_{m+1}), V(t_{m+1})\Big)\Big| \\
\le\ & 2\delta t\Big|\Big(W^m(\phi_t(t_{m+1}) - \phi_t^\star) + \Big(W(t_{m+1}) - W^m\Big)\phi_t(t_{m+1}) + e_B^{m+1}W^m\phi_t^\star, e_V^{m+1}\Big) \\
&+ e_B^{m+1}\Big(W^m\phi_t^\star, V^{m+1}\Big) - e_B^{m+1}\Big(W^m\phi_t^\star, V(t_{m+1})\Big) + e_B^{m+1}\Big(W^m\phi_t^\star, V(t_{m+1})\Big) \\
&- e_B^{m+1}\Big(W(t_{m+1})\phi_t(t_{m+1}), V(t_{m+1})\Big)\Big| \\
\le\ & 2\delta t\Big|\Big(W^m(\phi_t(t_{m+1}) - \phi_t^\star) + \Big(W(t_{m+1}) - W^m\Big)\phi_t(t_{m+1}) + e_B^{m+1}W^m\phi_t^\star, e_V^{m+1}\Big) \\
&+ e_B^{m+1}\Big(-\Big(W^m\phi_t^\star, e_V^{m+1}\Big) + \Big(W^m\phi_t^\star - W(t_{m+1})\phi_t(t_{m+1}), V(t_{m+1})\Big)\Big)\Big| \\
\le\ & 2\delta t\Big|\Big(W^m(\phi_t(t_{m+1}) - \phi_t^\star) + \Big(W(t_{m+1}) - W^m\Big)\phi_t(t_{m+1}), e_V^{m+1}\Big) \\
&+ e_B^{m+1}\Big(W^m\phi_t^\star - W(t_{m+1})\phi_t(t_{m+1}), V(t_{m+1})\Big)\Big| \\
\lesssim\ & \delta t\Big(\Big(\|W^m\|_{L^\infty}\|\phi_t(t_{m+1}) - \phi_t^\star\| + \|W(t_{m+1}) - W^m\|\|\phi_t(t_{m+1})\|_{L^\infty}\Big)\|e_V^{m+1}\| \\
&+ |e_B^{m+1}|\Big(\|W^m\|_{L^\infty}\|\phi_t^\star\|_{L^\infty} - \|W(t_{m+1})\|_{L^\infty}\|\phi_t(t_{m+1})\|_{L^\infty}\Big)\|V(t_{m+1})\|_{L^\infty}\Big) \\
\lesssim\ & \delta t\Big(\delta t^2 + \frac{1}{5}\|\Delta e_\mu^m\|^2 + \|e_\phi^m\|^2 + \|e_V^{m+1}\|^2 + |e_B^{m+1}|^2\Big),
\end{aligned} \tag{3.40}$$

$$
\begin{aligned}
|\mathbf{I_5}| &= \Big|2\delta t e_B^{m+1}\Big(W(t_{m+1})V(t_{m+1}), \phi_t(t_{m+1})\Big) - 2\delta t e_B^{m+1}\Big(W^m V^m, \frac{\phi^{m+1}-\phi^m}{\delta t}\Big)\Big| \\
&= \Big|2\delta t e_B^{m+1}\Big(W(t_{m+1})V(t_{m+1}) - W^m V^m, \phi_t(t_{m+1})\Big) \\
&\quad + 2\delta t e_B^{m+1}\Big(W^m V^m, \phi_t(t_{m+1}) - \frac{\phi^{m+1}-\phi^m}{\delta t} + \frac{\phi(t_{m+1})-\phi(t_m)}{\delta t} - \frac{\phi(t_{m+1})-\phi(t_m)}{\delta t}\Big)\Big| \\
&= \Big|2\delta t e_B^{m+1}\Big(W(t_{m+1})(V(t_{m+1}) - V^m) + (W(t_{m+1}) - W^m)V^m, \phi_t(t_{m+1})\Big) \\
&\quad + 2\delta t e_B^{m+1}\Big(W^m V^m, R_1^{m+1} + \frac{e_\phi^{m+1}-e_\phi^m}{\delta t}\Big)\Big| \\
&= \Big|2\delta t e_B^{m+1}\Big(W(t_{m+1})(V(t_{m+1}) - V^m) + (W(t_{m+1}) - W^m)V^m, \phi_t(t_{m+1})\Big) \\
&\quad + 2\delta t e_B^{m+1}\Big(W^m V^m, \Delta e_\mu^{m+1}\Big)\Big| \\
&\lesssim \delta t|e_B^{m+1}| \cdot \Big(\|V(t_{m+1}) - V^m\| + \|W(t_{m+1}) - W^m\| + \|\Delta e_\mu^{m+1}\|\Big) \\
&\lesssim \delta t\Big(\delta t^2 + |e_B^{m+1}|^2 + \|e_\phi^m\|^2 + \frac{1}{5}\|\Delta e_\mu^{m+1}\|^2\Big),
\end{aligned} \tag{3.41}
$$

$$
\begin{aligned}
|\mathbf{I_6}| &= \Big|2\Big(B(t_{m+1})W(t_{m+1})V(t_{m+1}) - B^{m+1}W^m V^m, \Delta(e_\phi^{m+1} - e_\phi^m)\Big)\Big| \\
&= 2\delta t\Big|\Big(\Delta(B(t_{m+1})W(t_{m+1})V(t_{m+1}) - B^{m+1}W^m V^m), \Delta e_\mu^{m+1} - R_1^{m+1}\Big)\Big| \\
&\lesssim \delta t\Big(\delta t^2 + |e_B^{m+1}|^2 + \|\Delta e_\phi^m\| + \frac{1}{5}\|\Delta e_\mu^{m+1}\|^2\Big).
\end{aligned} \tag{3.42}
$$

Substituting the estimates (3.27)–(3.33) and (3.37)–(3.42) into (3.26), we obtain

$$
\begin{aligned}
&\|L_1L_2e_\phi^{m+1}\|^2 - \|L_1L_2e_\phi^m\|^2 + \|L_1L_2(e_\phi^{m+1} - e_\phi^m)\|^2 \\
&\quad + r^2(\|L_1e_\phi^{m+1}\|^2 - \|L_1e_\phi^m\|^2 + \|L_1(e_\phi^{m+1} - e_\phi^m)\|^2) \\
&\quad + S(\|e_\phi^{m+1}\|^2 - \|e_\phi^m\|^2 + \|e_\phi^{m+1} - e_\phi^m\|^2) \\
&\quad + \|L_1^2(L_2^2 + r^2)e_\phi^{m+1}\|^2 - \|L_1^2(L_2^2 + r^2)e_\phi^m\|^2 + \|L_1^2(L_2^2 + r^2)(e_\phi^{m+1} - e_\phi^m)\|^2 \\
&\quad + S(\|L_1L_2e_\phi^{m+1}\|^2 - \|L_1L_2e_\phi^m\|^2 + \|L_1L_2(e_\phi^{m+1} - e_\phi^m)\|^2 \\
&\quad + r^2(\|L_1e_\phi^{m+1}\|^2 - \|L_1e_\phi^m\|^2 + \|L_1(e_\phi^m - e_\phi^{m+1})\|^2)) \\
&\quad + \|L_1L_2\nabla e_\phi^{m+1}\|^2 - \|L_1L_2\nabla e_\phi^m\|^2 + \|L_1L_2\nabla(e_\phi^{m+1} - e_\phi^m)\|^2 \\
&\quad + r^2(\|L_1\nabla e_\phi^{m+1}\|^2 - \|L_1\nabla e_\phi^m\|^2 + \|L_1\nabla(e_\phi^{m+1} - e_\phi^m)\|^2) \\
&\quad + S(\|\nabla e_\phi^{m+1}\|^2 - \|\nabla e_\phi^m\|^2 + \|\nabla(e_\phi^{m+1} - e_\phi^m)\|^2) \\
&\quad + 2(\|e_V^{m+1}\|^2 - \|e_V^m\|^2 + \|e_V^{m+1} - e_V^m\|^2) \\
&\quad + |e_B^{m+1}|^2 - |e_B^m|^2 + |e_B^{m+1} - e_B^m|^2 + 2\delta t\|\nabla e_\mu^{m+1}\|^2 + 2\delta t\|L_1L_2\nabla e_\mu^{m+1}\|^2 \\
&\quad + 2\delta t\|e_\mu^{m+1}\|^2 + 2r^2\delta t\|L_1\nabla e_\mu^{m+1}\|^2 + \delta t\|\Delta e_\mu^{m+1}\|^2 \\
&\lesssim \delta t(\|e_\phi^{m+1}\|^2 + \|e_\phi^m\|^2 + \|\Delta e_\phi^m\|^2 + \|e_V^{m+1}\|^2 + |e_B^{m+1}|^2 \\
&\quad + \|e_\mu^{m+1}\|^2 + \frac{4}{5}\|\Delta e_\mu^{m+1}\|^2 + \frac{1}{5}\|\Delta e_\mu^m\|^2 \\
&\quad + \|\nabla e_\mu^{m+1}\|^2 + \|L_1^2(L_2^2 + r^2)e_\phi^{m+1}\|^2 + \|L_1^2(L_2^2 + r^2)e_\phi^m\|^2) + \delta t^3.
\end{aligned} \tag{3.43}
$$

After dropping some nonessential positive terms on the left-hand side, we obtain

$$\begin{aligned}
&\|L_1L_2e_\phi^{m+1}\|^2 - \|L_1L_2e_\phi^m\|^2 + r^2(\|L_1e_\phi^{m+1}\|^2 - \|L_1e_\phi^m\|^2) + S(\|e_\phi^{m+1}\|^2 - \|e_\phi^m\|^2)\\
&\quad + 2(\|e_V^{m+1}\|^2 - \|e_V^m\|^2) + \|L_1^2(L_2^2 + r^2)e_\phi^{m+1}\|^2 - \|L_1^2(L_2^2 + r^2)e_\phi^m\|^2\\
&\quad + S(\|L_1L_2e_\phi^{m+1}\|^2 - \|L_1L_2e_\phi^m\|^2 + r^2(\|L_1e_\phi^{m+1}\|^2 - \|L_1e_\phi^m\|^2))\\
&\quad + \|L_1L_2\nabla e_\phi^{m+1}\|^2 - \|L_1L_2\nabla e_\phi^m\|^2 + r^2(\|L_1\nabla e_\phi^{m+1}\|^2 - \|L_1\nabla e_\phi^m\|^2)\\
&\quad + S(\|\nabla e_\phi^{m+1}\|^2 - \|\nabla e_\phi^m\|^2) + |e_B^{m+1}|^2 - |e_B^m|^2 + 2\delta t\|\nabla e_\mu^{m+1}\|^2\\
&\quad + 2\delta t\|L_1L_2\nabla e_\mu^{m+1}\|^2 + 2\delta t\|e_\mu^{m+1}\|^2 + 2r^2\delta t\|L_1\nabla e_\mu^{m+1}\|^2 + 2\delta t\|\Delta e_\mu^{m+1}\|^2\\
&\lesssim \delta t\Big(\|e_\phi^{m+1}\|^2 + \|e_\phi^m\|^2 + \|\Delta e_\phi^m\|^2 + \|e_V^{m+1}\|^2 + |e_B^{m+1}|^2 + \|e_\mu^{m+1}\|^2\\
&\quad + \frac{4}{5}\|\Delta e_\mu^{m+1}\|^2 + \frac{1}{5}\|\Delta e_\mu^m\|^2 + \|\nabla e_\mu^{m+1}\|^2 + \|L_1^2(L_2^2 + r^2)e_\phi^{m+1}\|^2\\
&\quad + \|L_1^2(L_2^2 + r^2)e_\phi^{m+1}\|^2\Big) + \delta t^3.
\end{aligned} \tag{3.44}$$

After collecting some terms and adding $\delta t(\|L_1L_2e_\phi^{m+1}\|^2 + \|L_1e_\phi^{m+1}\|^2 + \|L_1L_2\nabla e_\phi^{m+1}\|^2 + \|L_1\nabla e_\phi^{m+1}\|^2 + \|\nabla e_\phi^{m+1}\|^2)$ to the right-hand side, we obtain

$$\begin{aligned}
&(S+1)(\|L_1L_2e_\phi^{m+1}\|^2 - \|L_1L_2e_\phi^m\|^2 + r^2(\|L_1e_\phi^{m+1}\|^2 - \|L_1e_\phi^m\|^2))\\
&\quad + S\|e_\phi^{m+1}\|^2 - (S+1)\|e_\phi^m\|^2 + \|L_1^2(L_2^2 + r^2)e_\phi^{m+1}\|^2 - 2\|L_1^2(L_2^2 + r^2)e_\phi^m\|^2\\
&\quad + \|L_1L_2\nabla e_\phi^{m+1}\|^2 - \|L_1L_2\nabla e_\phi^m\|^2 + r^2(\|L_1\nabla e_\phi^{m+1}\|^2 - \|L_1\nabla e_\phi^m\|^2)\\
&\quad + S(\|\nabla e_\phi^{m+1}\|^2 - \|\nabla e_\phi^m\|^2)\\
&\quad + 2(\|e_V^{m+1}\|^2 - \|e_V^m\|^2) + |e_B^{m+1}|^2 - |e_B^m|^2 + \delta t\|\nabla e_\mu^{m+1}\|^2\\
&\quad + 2\delta t\|L_1L_2\nabla e_\mu^{m+1}\|^2 + \delta t\|e_\mu^{m+1}\|^2\\
&\quad + 2r^2\delta t\|L_1\nabla e_\mu^{m+1}\|^2 + \delta t\|\Delta e_\mu^{m+1}\|^2 + \frac{\delta t}{5}(\|\Delta e_\mu^{m+1}\|^2 - \|\Delta e_\mu^m\|^2)\\
&\lesssim \delta t\Big(\|e_\phi^{m+1}\|^2 + \|e_V^{m+1}\|^2 + |e_B^{m+1}|^2 + \|L_1^2(L_2^2 + r^2)e_\phi^{m+1}\|^2\\
&\quad + \|L_1L_2e_\phi^{m+1}\|^2 + \|L_1e_\phi^{m+1}\|^2 + \|L_1L_2\nabla e_\phi^{m+1}\|^2 + \|L_1\nabla e_\phi^{m+1}\|^2\\
&\quad + \|\nabla e_\phi^{m+1}\|^2\Big) + \delta t^3.
\end{aligned} \tag{3.45}$$

Summing the above equation over $m = 1, \cdots, n$, we arrive at

$$\begin{aligned}
&(S+1)\|L_1L_2e_\phi^{n+1}\|^2 + (S+1)r^2\|L_1e_\phi^{n+1}\|^2 + S\|e_\phi^{n+1}\|^2 + \|L_1^2(L_2^2 + r^2)e_\phi^{n+1}\|^2\\
&\quad + \|L_1L_2\nabla e_\phi^{n+1}\|^2 + r^2\|L_1\nabla e_\phi^{n+1}\|^2 + S\|\nabla e_\phi^{n+1}\|^2 + 2\|e_V^{n+1}\|^2 + |e_B^{n+1}|^2\\
&\quad + \delta t\sum_{m=1}^{n}\Big(\|\nabla e_\mu^{m+1}\|^2 + \|L_1L_2\nabla e_\mu^{m+1}\|^2 + \|e_\mu^{m+1}\|^2 + \|L_1\nabla e_\mu^{m+1}\|^2 + \|\Delta e_\mu^{m+1}\|^2\Big)\\
&\lesssim \delta t\sum_{m=0}^{n}\Big(\|e_\phi^{m+1}\|^2 + \|e_V^{m+1}\|^2 + |e_B^{m+1}|^2 + \|L_1^2(L_2^2 + r^2)e_\phi^{m+1}\|^2 + \|L_1L_2e_\phi^{m+1}\|^2\\
&\quad + \|L_1e_\phi^{m+1}\|^2 + \|L_1L_2\nabla e_\phi^{m+1}\|^2 + \|L_1\nabla e_\phi^{m+1}\|^2 + \|\nabla e_\phi^{m+1}\|^2\Big)\\
&\quad + \delta t^2 + \frac{\delta t}{5}\|\Delta e_\mu^1\|^2.
\end{aligned} \tag{3.46}$$

Adding $\delta t(\|\nabla e_\mu^1\|^2+\|L_1L_2\nabla e_\mu^1\|^2+\|e_\mu^1\|^2+\|L_1\nabla e_\mu^1\|^2+\|\Delta e_\mu^1\|^2)$ to both sides of the above inequality yields

$$\begin{aligned}
&(S+1)\|L_1L_2e_\phi^{n+1}\|^2+(S+1)r^2\|L_1e_\phi^{n+1}\|^2+S\|e_\phi^{n+1}\|^2+\|L_1^2(L_2^2+r^2)e_\phi^{n+1}\|^2\\
&\quad+\|L_1L_2\nabla e_\phi^{n+1}\|^2+r^2\|L_1\nabla e_\phi^{n+1}\|^2+S\|\nabla e_\phi^{n+1}\|^2+2\|e_V^{n+1}\|^2+|e_B^{n+1}|^2\\
&\quad+\delta t\sum_{m=0}^{n}\left(\|\nabla e_\mu^{m+1}\|^2+\|L_1L_2\nabla e_\mu^{m+1}\|^2+\|e_\mu^{m+1}\|^2+\|L_1\nabla e_\mu^{m+1}\|^2+\|\Delta e_\mu^{m+1}\|^2\right)\\
&\lesssim\delta t\sum_{m=0}^{n}\left(\|e_\phi^{m+1}\|^2+\|e_V^{m+1}\|^2+|e_B^{m+1}|^2+\|L_1^2(L_2^2+r^2)e_\phi^{m+1}\|^2\right.\\
&\quad\left.+\|L_1L_2e_\phi^{m+1}\|^2+\|L_1e_\phi^{m+1}\|^2+\|L_1L_2\nabla e_\phi^{m+1}\|^2+\|L_1\nabla e_\phi^{m+1}\|^2+\|\nabla e_\phi^{m+1}\|^2\right)\\
&\quad+\delta t(\|\nabla e_\mu^1\|^2+\|L_1L_2\nabla e_\mu^1\|^2+\|e_\mu^1\|^2+\|L_1\nabla e_\mu^1\|^2+\frac{6}{5}\|\Delta e_\mu^1\|^2)+\delta t^2.
\end{aligned}\tag{3.47}$$

For the first step ($n=0$), we obtain a similar result as

$$\begin{aligned}
&(S+1)\|L_1L_2e_\phi^1\|^2+(S+1)r^2\|L_1e_\phi^1\|^2+S\|e_\phi^1\|^2+\|L_1^2(L_2^2+r^2)e_\phi^1\|^2\\
&\quad+2\|e_V^1\|^2+\|L_1L_2\nabla e_\phi^1\|^2+r^2\|L_1\nabla e_\phi^1\|^2+S\|\nabla e_\phi^1\|^2+|e_B^1|^2\\
&\quad+\delta t(\|\nabla e_\mu^1\|^2+\|L_1L_2\nabla e_\mu^1\|^2+\|e_\mu^1\|^2+\|L_1\nabla e_\mu^1\|^2+\|\Delta e_\mu^1\|^2)\\
&\quad\lesssim\delta t(\delta t^2+\|e_V^1\|^2+|e_B^1|^2).
\end{aligned}\tag{3.48}$$

To obtain a uniform bound for ϕ^1, we split the above estimate into two parts: there exist constants C_2 and C_3 such that

$$\begin{aligned}
&(S+1)\|L_1L_2e_\phi^1\|^2+(S+1)r^2\|L_1e_\phi^1\|^2+S\|e_\phi^1\|^2+\|L_1^2(L_2^2+r^2)e_\phi^1\|^2\\
&\quad+\|L_1L_2\nabla e_\phi^1\|^2+r^2\|L_1\nabla e_\phi^1\|^2+S\|\nabla e_\phi^1\|^2\le C_2\delta t^3,
\end{aligned}\tag{3.49}$$

and

$$\|\nabla e_\mu^1\|^2+\|L_1L_2\nabla e_\mu^1\|^2+\|e_\mu^1\|^2+\|L_1\nabla e_\mu^1\|^2+\|\Delta e_\mu^1\|^2\le C_3\delta t^2.\tag{3.50}$$

Then

$$\begin{aligned}
\|\phi^1\|_{L^\infty}&\le\|e_\phi^1\|_\infty+\|\phi(t_1)\|_{L^\infty}\\
&\le C_\Omega\|e_\phi^1\|_{H^1}^{\frac12}\|e_\phi^1\|_{H^2}^{\frac12}+\|\phi(t_1)\|_{L^\infty}\\
&\le C_\Omega\sqrt{C_2}\delta t^{\frac32}+\|\phi(t_1)\|_{L^\infty}.
\end{aligned}\tag{3.51}$$

If $C_\Omega\sqrt{C_2}\delta t^{\frac32}\le 1$, i.e., $\delta t\le(\frac{1}{C_\Omega\sqrt{C_2}})^{\frac23}$, it holds that

$$\|\phi^1\|_{L^\infty}\le 1+\|\phi(t_1)\|_{L^\infty}\le G^*.\tag{3.52}$$

Combining (3.47) with the estimate (3.50) and applying the discrete Gronwall inequality, we obtain that there exists positive constants C_4, C_5, independent of δt, such that, when $\delta t\le C_4$, we have

$$\begin{aligned}
&(S+1)\|L_1L_2e_\phi^{n+1}\|^2+(S+1)r^2\|L_1e_\phi^{n+1}\|^2+S\|e_\phi^{n+1}\|^2+\|L_1^2(L_2^2+r^2)e_\phi^{n+1}\|^2\\
&\quad+\|L_1L_2\nabla e_\phi^{n+1}\|^2+r^2\|L_1\nabla e_\phi^{n+1}\|^2+S\|\nabla e_\phi^{n+1}\|^2+2\|e_V^{n+1}\|^2+|e_B^{n+1}|^2\\
&\quad+\delta t\sum_{m=0}^{n}\left(\|\nabla e_\mu^{m+1}\|^2+\|L_1L_2\nabla e_\mu^{m+1}\|^2+\|e_\mu^{m+1}\|^2+\|L_1\nabla e_\mu^{m+1}\|^2+\|\Delta e_\mu^{m+1}\|^2\right)\\
&\quad\le C_5\delta t^2.
\end{aligned}\tag{3.53}$$

Hence, we have

$$\begin{aligned}\|\phi^{n+1}\|_{L^\infty} &\le \|e_\phi^{n+1}\|_\infty + \|\phi(t_{n+1})\|_{L^\infty} \\ &\le C_\Omega \|e_\phi^{n+1}\|_{H^1}^{\frac{1}{2}} \|e_\phi^{n+1}\|_{H^2}^{\frac{1}{2}} + \|\phi(t_{n+1})\|_{L^\infty} \\ &\le C_\Omega \sqrt{C_5}\delta t + \|\phi(t_{n+1})\|_{L^\infty}. \end{aligned} \tag{3.54}$$

If $C_\Omega \sqrt{C_5}\delta t \le 1$, i.e., $\delta t \le \frac{1}{C_\Omega \sqrt{C_5}}$, we can get

$$\|\phi^{n+1}\|_{L^\infty} \le 1 + \|\phi(t_{n+1})\|_{L^\infty} \le G^*. \tag{3.55}$$

By choosing $\delta t \le \tau_0 = \min\left\{C_2, \left(\frac{1}{C_\Omega \sqrt{C_2}}\right)^{\frac{2}{3}}, C_4, \frac{1}{C_\Omega \sqrt{C_5}}\right\}$, we get the conclusion.

Theorem 3.1. *Under the assumptions of Lemma 3.2, the following temporal error estimate holds:*

$$\|\phi(t_{n+1}) - \phi^{n+1}\|_{H^2}^2 + \|V(t_{n+1}) - V^{n+1}\|^2 + |B(t_{n+1}) - B^{n+1}|^2 \lesssim \delta t^2.$$

Proof. Given that $\|\phi^n\|_{L^\infty} \le G^*$ is satisfied for all $n = 0, \cdots, T/\delta t - 1$ the conclusion of the theorem follows directly by applying the procedure outlined in Lemma 3.2.

4. Numerical examples

Following the theoretical results given in the previous section, we now present a set of numerical examples to verify the predicted temporal accuracy, confirm the discrete energy-dissipation property, and illustrate the performance of the proposed scheme for two- and three-dimensional crystallization problems. All simulations are carried out on periodic domains of the form $[0, L]^d$ (with $d = 2, 3$). We use a Fourier spectral method for spatial discretization. In Fourier space, the constant-coefficient elliptic operators become diagonal, so the linear systems at each time step can be solved efficiently by direct division for each Fourier mode. In the tests below, the spatial mesh is chosen fine enough so that the temporal error dominates, unless stated otherwise.

4.1. Temporal accuracy tests

We first consider a manufactured-solution test on a two-dimensional domain and set the model parameters as

$$L_2 = 1, S = 1, M = 1, A = 1, \epsilon = 0.5, q = \sqrt{2}, r = 3, \lambda = 0.001,$$

(we refer the parameters settings to [22, 30].) To assess the temporal accuracy, we prescribe the exact solution

$$\phi(\boldsymbol{x}, t) = \sin(\pi x)\cos(\pi y)\cos(t),$$

and add a suitable forcing term so that ϕ solves the modified PFC-FCC system exactly. The auxiliary variables V and B are then defined consistently from ϕ via (2.8)–(2.10). In this test, we fix the spatial mesh and vary only the time step δt, so that the observed errors mainly reflect the temporal accuracy of the scheme.

The errors are measured at $T = 1$ by comparing the numerical solutions of ϕ, V , and B with their corresponding exact values. Figure 1 shows the L^2 errors of ϕ and V, together with the absolute error of B from its exact value 1, in a log-log plot as functions of the time step. All three variables exhibit a first-order decay with respect to δt, which agrees with the theoretical analysis.

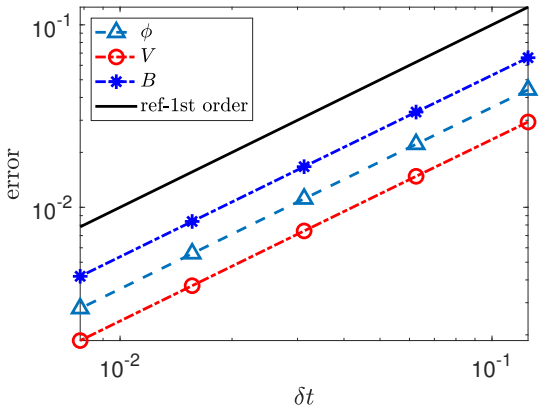

Figure 1. L^2 errors of ϕ and V and absolute error of B, illustrating first-order temporal convergence.

4.2. Sensitivity analysis

To investigate the sensitivity of the problem with respect to key parameters, we perform a sensitivity analysis based on Section 4.1 and the control variable method. Figure 2(a) shows the L^2 errors of ϕ for different values of $M = 1, 10, 40$ with $S = 1$ fixed. Figure 2(b) presents the L^2 errors of ϕ for different values of $S = 1, 10, 40$ with $M = 1$ fixed.

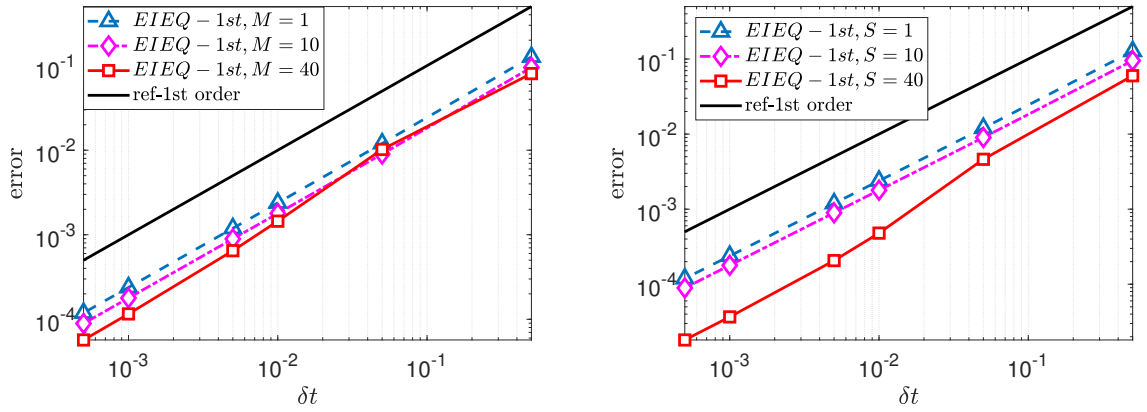

(a) For the parameter M.

(b) For the parameter S.

Figure 2. Sensitivity analysis of (2.18)–(2.21) with respect to different values of M and S.

4.3. 2D Phase transition

When a molten metal cools and solidifies, its atoms rearrange from a disordered liquid-like state to ordered crystalline patterns. Different crystal packings, such as BCC and FCC, may nucleate and compete during this process, and the mixture of these structures and the finally selected dominant phase have a strong impact on the material's mechanical properties. In particular, controlling whether a material solidifies predominantly in a BCC or FCC structure is closely related to tuning its strength, ductility, and resistance to deformation in alloy design. To mimic this kind of solidification and to show that our scheme can resolve the associated microstructure formation and phase selection, we perform a two-dimensional simulation of the PFC-FCC model.

The computational domain is $\bar{\Omega} = [0, 256]^2$ with spatial mesh size $h = 1$ and time step $\delta t = 0.1$. As an initial condition, we choose

$$\phi|_{t=0} = \phi_0 + 0.01\text{rand}(x, y), \tag{4.1}$$

where $\text{rand}(x, y)$ denotes a random number uniformly distributed in $[0, 1]$ at each grid point. This corresponds to an almost homogeneous state with small-amplitude random fluctuations. Physically, one may think of a liquid or weakly ordered solid that has just been quenched into a parameter regime where the uniform state is unstable with respect to the formation of close-packed density waves. The random perturbation plays the role of thermal noise: it seeds crystallization at many locations and in many orientations, without imposing any preferred lattice structure by hand, so that the subsequent BCC/FCC pattern selection is determined by the model dynamics.

For the parameter set $\epsilon = 0.195$ and $\phi_0 = 0.23$, the simulation exhibits a clear sequence of pattern-formation stages, as illustrated in Figure 3. At $t = 20$, the field ϕ is close to its noisy initial state and only small, irregular fluctuations are visible. By $t = 100$, numerous small crystalline nuclei have formed throughout the domain. At $t = 400$, these nuclei have grown into larger clusters, and patches with locally ordered structures begin to emerge. At intermediate times $t = 700$ and $t = 1000$, domains with BCC-like packing and domains with nearly FCC ordering coexist and compete, and a complex network of grain boundaries separates these regions. By $t = 2000$, most of the domain has rearranged into a well-ordered close-packed pattern in which FCC ordering dominates, with only a few residual defects and grain boundaries remaining.

The corresponding time evolution of the free-energy functional, plotted in Figure 4(a), shows a rapid drop during the early nucleation and growth stages, followed by a slower decay associated with domain coarsening and grain-boundary motion. Overall, the free energy decreases monotonically in time, which agrees with the theoretical energy-dissipation property of the PFC–FCC model and is consistent with other studies [9, 22]. This example indicates that the proposed scheme can stably capture long-time solidification dynamics and the competition between different close-packed structures without introducing numerical artifacts.

Finally, Figure 4(b) demonstrates that the proposed scheme strictly preserves mass conservation and maintains a monotonically non-increasing discrete energy. The computational cost for a single time step on a 256×256 mesh is approximately 0.35 seconds, as the method decouples into solving several independent constant-coefficient bi-Laplace equations.

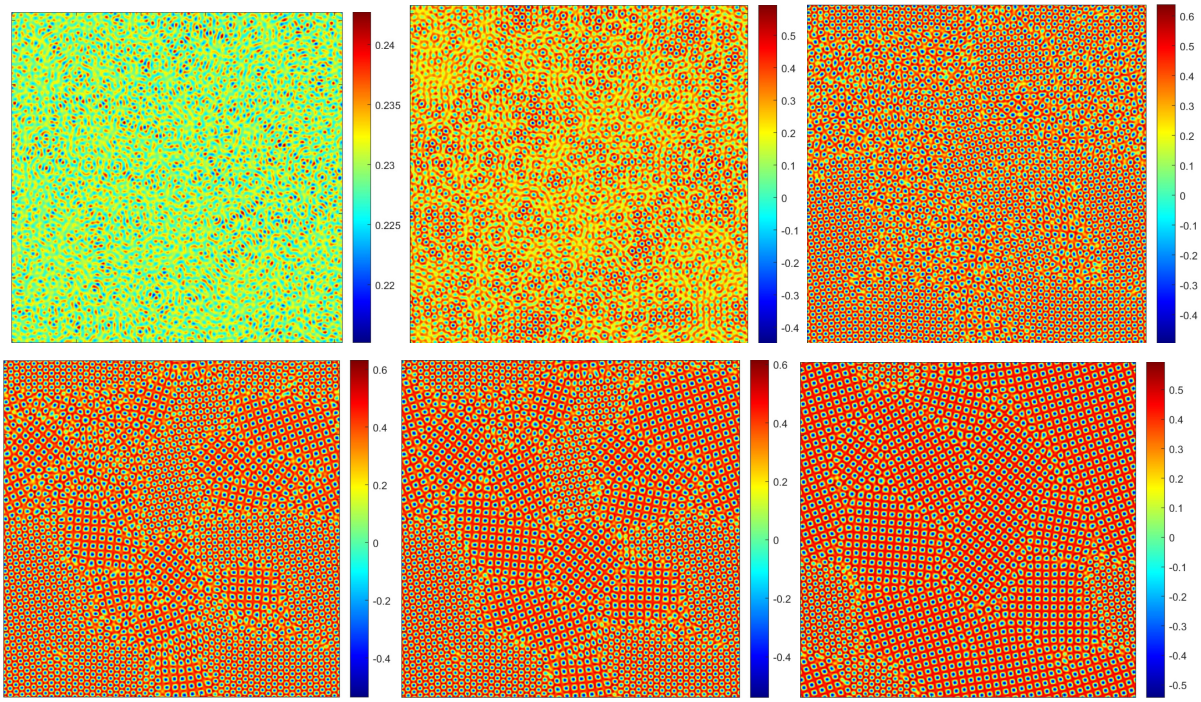

Figure 3. 2D phase transition: Snapshots of the phase-field variable ϕ at times $t = 20, 100, 400, 700, 1000$, and 2000 with $\delta t = 0.1$. The color represents the local density modulation, whose peaks indicate likely atomic positions. The images show how an initially disordered, liquid-like state gradually develops crystalline nuclei, passes through mixed BCC/FCC microstructures, and evolves into a configuration dominated by FCC ordering.

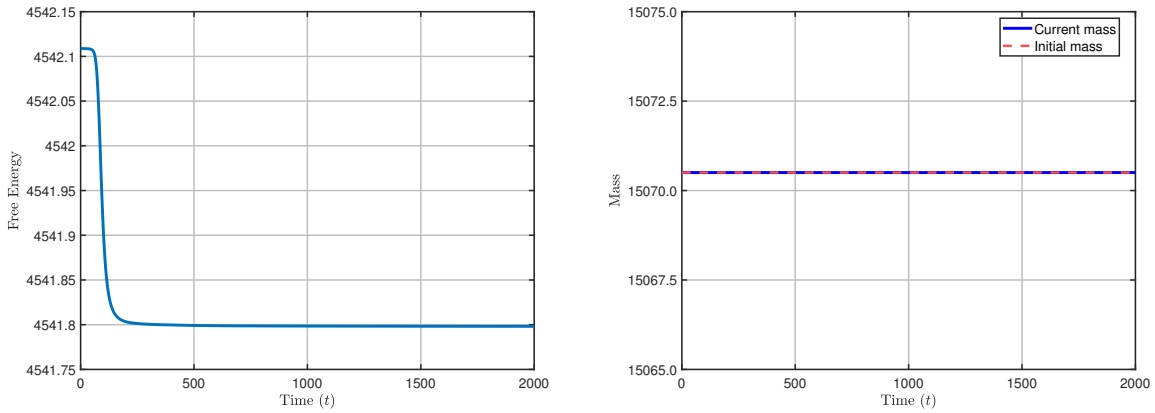

(a) (b)

Figure 4. Time history of the normalized energy and mass.

4.4. 3D Crystallization

When a supercooled liquid contains a small crystalline seed, the surrounding atoms may gradually rearrange so that the crystal grows into the melt. The geometry, orientation, and final shape of such growing crystallites are closely related to the material's microstructure and hence to its macroscopic properties. Three-dimensional simulations that resolve this process are therefore an important test for any numerical method intended for PFC-type models. In particular, they enable us to check whether the scheme can handle fully 3D close-packed structures, capture the growth of an embedded crystal, and remain stable over long time intervals on relatively fine grids.

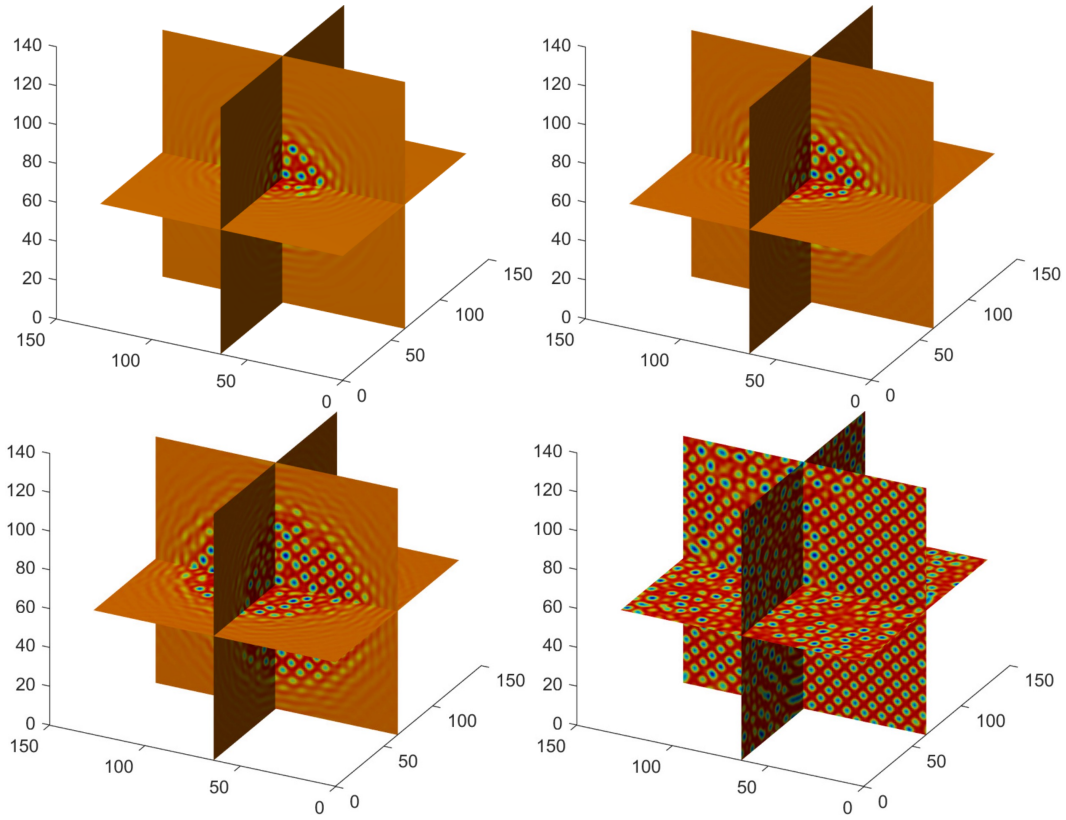

Figure 5. 3D crystallization of a micro-crystal: Snapshots of the phase-field variable ϕ at representative times $t = 600, 800, 1200$, and 6000 with $\delta t = 0.1$. The three orthogonal cut-planes visualize the internal density modulation. The images illustrate the growth of an initially localized crystallite embedded in a supercooled liquid into a fully developed three-dimensional structure with pronounced FCC ordering.

We therefore consider the three-dimensional crystallization of a single micro-crystal embedded in a supercooled liquid background. The computational domain is taken as $\bar{\Omega} = [0, 100]^3$, discretized by $129 \times 129 \times 129$ Fourier modes. The initial condition is chosen as a small crystallite surrounded by

a nearly uniform liquid state,

$$\phi(x, y, z, t)|_{t=0} = \phi_0 + G(\cos(b_1 y)\cos(ax) + \cos(b_2 z)\cos(ax) + \cos(b_1 y)\cos(b_2 z) - 0.5\cos(b_1 y)), \quad (4.2)$$

where $\phi_0 = -0.015$, $G = 0.15$, $a = 0.66$, $b_1 = 0.38$, and $b_2 = 0.46$. This modulation represents a localized region with FCC-like ordering embedded in a liquid-like background. The model parameters are set as $M = 1$, $q = \sqrt{2}$, $r = 0$, and $S = 2$, corresponding to a regime in which FCC order is energetically favored.

Figure 5 shows the numerical solution at several representative times. The three mutually orthogonal cut-planes visualize the density modulation ϕ inside the bulk. At early times ($t = 600$), the crystalline seed is relatively small and is surrounded by a nearly uniform liquid. As time evolves to $t = 800$ and $t = 1200$, the crystal grows outward in all directions, with the density peaks arranging themselves into a 3D close-packed pattern. At later times ($t = 6000$), the crystallite has expanded into a much larger region and develops a well-defined 3D structure with pronounced FCC ordering; the internal layers and stacking sequence become visible in the cross-sections. This example demonstrates that the proposed scheme can robustly simulate the growth of a three-dimensional FCC crystal from a small seed, while resolving the detailed atomic-scale morphology and orientation of the resulting microstructure, which is essential for applications to microstructure evolution in metallic and soft-matter systems. In practice, such "virtual solidification experiments" can be used as a cheap numerical testbed to explore how changes in alloy parameters or cooling conditions affect the shape and internal structure of growing crystals, and hence the strength and ductility of the final material.

5. Conclusions

In this work, we investigate a linear time-discretization scheme for solving the standard two-mode phase-field crystal model describing FCC ordering. Within the EIEQ framework, we introduce one auxiliary field and one scalar nonlocal variable to rewrite the original model into an equivalent system that preserves an energy-dissipation law at the continuous level. On this basis, we design a fully decoupled time-marching scheme that, at each time step, requires only the solution of constant-coefficient elliptic problems together with a scalar update. We prove unique solvability, unconditional energy stability, and optimal first-order temporal error estimates under suitable regularity assumptions. A key ingredient of the error analysis is a uniform L^∞-bound, obtained by combining the discrete energy law with the structure of the quadratized free energy, which enables us to control the nonlinear terms and close the Gronwall argument. Numerical tests confirm the theoretical convergence rate, and 2D/3D simulations of FCC ordering and crystallization show monotone decay of the discrete free energy as well as physically reasonable pattern-selection dynamics between BCC and FCC structures, demonstrating robust and accurate behavior of the developed EIEQ scheme.

From a broader perspective, the proposed method can be viewed as efficient "numerical laboratories" for studying long-time microstructure evolution in close-packed alloys. Future directions include the design and analysis of higher-order EIEQ-based schemes (for example, second-order BDF or Runge–Kutta variants), the derivation of fully discrete error estimates that incorporate spatial discretization (e.g., Fourier spectral or finite element methods), and the extension of the framework to multicomponent PFC-type models and more complex crystal symmetries.

Use of AI tools declaration

The authors declare they have not used Artificial Intelligence (AI) tools in the creation of this article.

Acknowledgements

The work of J. Zhang is supported by the National Natural Science Foundation of China (No. 12261017) and the Science and Technology Foundation of Guizhou Province (No. ZD[2026]004), and the Postgraduate program of Guizhou University of Finance and Economics (No. 2025BAZYSY214).

Conflict of interest

The authors declare there are no conflicts of interest.

References

1. K. R. Elder, M. Grant, Modeling elastic and plastic deformations in nonequilibrium processing using phase-field crystals, *Phys. Rev. E*, **70** (2004), 051605. https://doi.org/10.1103/PhysRevE.70.051605
2. K. R. Elder, M. Katakowski, M. Haataja, M. Grant, Modeling elasticity in crystal growth, *Phys. Rev. Lett.*, **88** (2002), 245701. https://doi.org/10.1103/PhysRevLett.88.245701
3. H. Emmerich, H. Löwen, R. Wittkowski, T. Gruhn, G. I. Tóth, G. Tegze, et al., Phase-field-crystal models for condensed matter dynamics on atomic length and diffusive time scales: An overview, *Adv. Phys.*, **61** (2012), 665–743. https://doi.org/10.1080/00018732.2012.737555
4. Z. Guan, V. Heinonen, J. Lowengrub, C. Wang, S. Wise, An energy stable, hexagonal finite difference scheme for the 2D phase field crystal amplitude equations, *J. Comput. Phys.*, **321** (2016), 1026–1054. https://doi.org/10.1016/j.jcp.2016.06.007
5. Y. Li, C. Luo, B. Xia, J. Kim, An efficient linear second order unconditionally stable direct discretization method for the phase-field crystal equation on surfaces, *Appl. Math. Model.*, **67** (2019), 477–490. https://doi.org/10.1016/j.apm.2018.11.012
6. M. Dehghan, V. Mohammadi, The numerical simulation of the phase field crystal (PFC) and modified phase field crystal (MPFC) models via global and local meshless methods, *Comput. Methods Appl. Mech. Eng.*, **298** (2016), 453–484. https://doi.org/10.1016/j.cma.2015.09.018
7. M. Wang, Q. Huang, C. Wang, A second order accurate scalar auxiliary variable (SAV) numerical method for the square phase field crystal equation, *J. Sci. Comput.*, **88** (2021), 33. https://doi.org/10.1007/s10915-021-01487-y
8. J. Yang, J. Kim, Numerical approximation of the square phase-field crystal dynamics on the three-dimensional objects, *J. Comput. Phys.*, **471** (2022), 111652. https://doi.org/10.1016/j.jcp.2022.111652
9. K. Wu, A. Adland, A. Karma, Phase-field-crystal model for fcc ordering, *Phys. Rev. E*, **81** (2010), 061601. https://doi.org/10.1103/PhysRevE.81.061601

10. G. I. Tóth, G. Tegze, T. Pusztai, G. Tóth, L. Gránásy, Polymorphism, crystal nucleation and growth in the phase-field crystal model in 2d and 3d, *J. Phys.: Condens. Matter*, **22** (2010), 364101. https://doi.org/10.1088/0953-8984/22/36/364101

11. S. Tang, R. Backofen, J. Wang, Y. Zhou, A. Voigt, Y. Yu, Three-dimensional phase-field crystal modeling of fcc and bcc dendritic crystal growth, *J. Cryst. Growth*, **334** (2011), 146–152. https://doi.org/10.1016/j.jcrysgro.2011.08.027

12. E. Asadi, M. A. Zaeem, Quantifying a two-mode phase-field crystal model for bcc metals at melting point, *Comput. Mater. Sci.*, **105** (2015), 101–109. https://doi.org/10.1016/j.commatsci.2015.03.051

13. E. Asadi, M. A. Zaeem, A modified two-mode phase-field crystal model applied to face-centered cubic and body-centered cubic orderings, *Comput. Mater. Sci.*, **105** (2015), 110–113. https://doi.org/10.1016/j.commatsci.2015.04.004

14. V. Ankudinov, P. K. Galenko, The diagram of phase-field crystal structures: An influence of model parameters in a two-mode approximation, *IOP Conf. Ser.: Mater. Sci. Eng.*, **192** (2017), 012019. https://doi.org/10.1088/1757-899X/192/1/012019

15. E. Asadi, M. A. Zaeem, Quantitative phase-field crystal modeling of solid-liquid interfaces for FCC metals, *Comput. Mater. Sci.*, **127** (2017), 236–243. https://doi.org/10.1016/j.commatsci.2016.11.005

16. S. M. Wise, C. Wang, J. S. Lowengrub, An energy-stable and convergent finite-difference scheme for the phase field crystal equation, *SIAM J. Numer. Anal.*, **47** (2009), 2269–2288. https://doi.org/10.1137/080738143

17. A. Baskaran, J. S. Lowengrub, C. Wang, S. M. Wise, Convergence analysis of a second order convex splitting scheme for the modified phase field crystal equation, *SIAM J. Numer. Anal.*, **51** (2013), 2851–2873. https://doi.org/10.1137/120880677

18. Q. Li, N. Cui, S. Zheng, L. Mei, A new Allen-Cahn type two-model phase-field crystal model for fcc ordering and its numerical approximation, *Appl. Math. Lett.*, **132** (2022), 108211. https://doi.org/10.1016/j.aml.2022.108211

19. Z. Tan, L. Chen, J. Yang, Generalized Allen-Cahn-type phase-field crystal model with FCC ordering structure and its conservative high-order accurate algorithm, *Comput. Phys. Commun.*, **286** (2023), 108656. https://doi.org/10.1016/j.cpc.2023.108656

20. Y. Ye, X. Feng, L. Qian, A second-order strang splitting scheme for the generalized Allen-Cahn type phase-field crystal model with FCC ordering structure, *Commun. Nonlinear Sci. Numer. Simul.*, **137** (2024), 108143. https://doi.org/10.1016/j.cnsns.2024.108143

21. X. Yang, D. Han, Linearly first- and second-order, unconditionally energy stable schemes for the phase field crystal equation, *J. Comput. Phys.*, **330** (2017), 1116–1134. https://doi.org/10.1016/j.jcp.2016.10.020

22. Z. Zhang, X. Yang, On efficient numerical schemes for a two-mode phase field crystal model with face-centered-cubic (FCC) ordering structure, *Appl. Numer. Math.*, **146** (2019), 13–37. https://doi.org/10.1016/j.apnum.2019.06.017

23. Y. Ye, Q. Li, L. Mei, W. Wang, A variable-step, structure-preserving and linear fully discrete scheme for the two-mode phase-field crystal model with face-centered-cubic ordering, *Commun. Nonlinear Sci. Numer. Simul.*, **146** (2025), 108766. https://doi.org/10.1016/j.cnsns.2025.108766

24. Z. Xu, X. Yang, H. Zhang, Z. Xie, Efficient and linear schemes for anisotropic Cahn–Hilliard model using the Stabilized-Invariant Energy Quadratization (S-IEQ) approach, *Comput. Phys. Commun.*, **238** (2019), 36–49. https://doi.org/10.1016/j.cpc.2018.12.019

25. J. Zhang, X. Yang, Unconditionally energy stable large time stepping method for the L2-gradient flow based ternary phase-field model with precise nonlocal volume conservation, *Comput. Methods Appl. Mech. Eng.*, **361** (2020), 112743. https://doi.org/10.1016/j.cma.2019.112743

26. J. Zhang, C. Chen, X. Yang, A novel decoupled and stable scheme for an anisotropic phase-field dendritic crystal growth model, *Appl. Math. Lett.*, **95** (2019), 122–129. https://doi.org/10.1016/j.aml.2019.03.029

27. G. D. Zhang, X. He, X. Yang, Decoupled, linear, and unconditionally energy stable fully discrete finite element numerical scheme for a two-phase ferrohydrodynamics model, *SIAM J. Sci. Comput.*, **43** (2021), B167–B193. https://doi.org/10.1137/19M1288280

28. X. Yang, Linear, first and second-order, unconditionally energy stable numerical schemes for the phase field model of homopolymer blends, *J. Comput. Phys.*, **327** (2016), 294–316. https://doi.org/10.1016/j.jcp.2016.09.029

29. X. Yang, X. He, Numerical approximations of flow coupled binary phase field crystal system: Fully discrete finite element scheme with second-order temporal accuracy and decoupling structure, *J. Comput. Phys.*, **467** (2022), 111448. https://doi.org/10.1016/j.jcp.2022.111448

30. J. Zhang, F. Song, X. Yang, Y. Zhang, Error analysis of the explicit-invariant energy quadratization (EIEQ) numerical scheme for solving the Allen-Cahn equation, *J. Comput. Appl. Math.*, **457** (2025), 116224. https://doi.org/10.1016/j.cam.2024.116224

AIMS Press